

BENDING MODE ACCELERATION INFLUENCE  
ON PILOT CONTROL OF FLEXIBLE  
BOOSTER DYNAMICS

by

PHILIP S. KILPATRICK

A.B., Carleton College  
(1964)

S.B., Massachusetts Institute of Technology  
(1964)

SUBMITTED IN PARTIAL FULFILLMENT  
OF THE REQUIREMENTS FOR THE  
DEGREE OF MASTER OF SCIENCE

at the

MASSACHUSETTS INSTITUTE OF TECHNOLOGY

September 1965

Signature of Author \_\_\_\_\_

Department of Aeronautics and  
Astronautics, September 1965

Certified by \_\_\_\_\_

Professor Laurence R. Young, Thesis Supervisor

Accepted by \_\_\_\_\_

Chairman, Departmental Graduate Committee



BENDING MODE ACCELERATION INFLUENCE  
ON PILOT CONTROL OF FLEXIBLE  
BOOSTER DYNAMICS

by

Philip S. Kilpatrick

Submitted to the Department of Aeronautics and Astronautics, Massachusetts Institute of Technology, on September 30, 1965, in partial fulfillment of the requirements for the degree of Master of Science.

ABSTRACT

This investigation is concerned with the general problem of man's ability to directly control a large flexible launch vehicle. Specifically, the effect of a flexible body mode on pilot control of simulated single axis Saturn V rigid body dynamics is studied. First bending mode amplitude and natural frequency, and the type of simulation, fixed or moving base, are the variables considered most intensively. Brief studies of variations in the RMS level of the disturbance signal and comparisons of two proposed control stick filters and vehicle augmentation schemes are included.

The effects of the flexible mode on the pilot and his closed loop performance are analyzed by ratios of attitude error to disturbance signal and control stick output to attitude error, and by computed pilot transfer functions.

Results show that pilot's ability to generate lead compensation and to control the attitude error decreased as the bending mode amplitude increased. Significant deterioration occurred at the lowest bending mode amplitude,  $1/3$  the value at the proposed location of the Saturn V attitude gyro, under study. The pilot's gain and ability to control the attitude error decreased during the moving base experiments. This result is attributed to dynamics and nonlinearities associated with the simulator, a less sensitive moving base display, and possibly vestibular uncertainty.

and insensitivity concerning small deflections from the vertical. With increasing bending mode amplitude, pilot performance deteriorates at approximately the same rate for both  $\omega_{nbd} = 5$  and 7 rad/sec. However, for a given amplitude, the 5 rad/sec bending mode generates only one-half the acceleration of the 7 rad/sec bending mode.

Thesis Supervisor: Laurence R. Young

Title: Assistant Professor of Aeronautics and Astronautics

ACKNOWLEDGEMENTS

The author wishes to thank Professor L. R. Young, his thesis advisor, for stimulating initial interest in the problem and for offering guidance throughout the research.

Professor J. L. Meiry's instructions concerning operation of the Man-Vehicle Control Laboratory's NE-2 Motion Simulator and assistance with digital computer aspects of the data analysis are gratefully acknowledged.

Mr. Ernest Silagyi prepared the computer program to transform data from analog to digital form. This work was completed on the Electrical Engineering Department's TX-0 Computer.

The M.I.T. Computation Center granted time on its IBM 7094 Computer for work done as Problems M4345 and M4347.

The author also expresses his thanks to Miss Toni Mello for typing the thesis.

This research was supported by NASA Grant NsG-577.

TABLE OF CONTENTS

		<u>Page No.</u>
Chapter I	Introduction	1
Chapter II	Simulation and Equipment	6
Chapter III	Procedure	12
Chapter IV	Discussion of Results	16
Chapter V	Conclusions	30
Appendix A	Derivation and Simplification of Simulation Equations	33
Appendix B	Pilot Describing Function Measure- ment Technique	42
Bibliography		45
Fig. 1	General block diagram for the man- booster control problem.	46
Fig. 2	Block diagram for the man-booster control problem showing components used in this investigation.	47
Fig. 3	Analog computer patching program for fixed base experiments.	48
Fig. 4	Analog computer patching program for moving base experiments.	49
Fig. 5	Analog computer patching program for a modified version of the augmented dynamics and stick filter recommended by Jex and Teper.	50

		<u>Page No.</u>
Fig. 6	Analog computer patching program used to shape the spectrum of the disturbance signal.	51
Fig. 7	NE-2 motion simulator.	52
Fig. 8	Fixed and moving base control stick characteristics.	53
Fig. 9	Block diagram showing control systems signals recorded on strip chart and tape recorders.	54
Fig. 10	Subject position and equipment location for fixed base experiments.	55
Fig. 11	Subject position, control stick, and display location for moving base experiments.	56
Fig. 12	Analog computer patching program for integral square error calculations.	57
Fig. 13	Strip chart recordings of attitude error	58
Fig. 14	Strip chart recordings of pilot response	59
Table 1	Transfer function data for fixed base session, $\omega_{nbd} = 5$ rad/sec.	60
Table 2	Transfer function data for fixed base session, $\omega_{nbd} = 7$ rad/sec.	61
Table 3	Transfer function data for moving base session, $\omega_{nbd} = 7$ rad/sec.	62
Table 4	Transfer function data for moving base session, $\omega_{nbd} = 5$ rad/sec.	63
Fig. 15	Plot of amplitude ratio data from Table 1.	64
Fig. 16	Plot of amplitude ratio data from Table 2.	65
Fig. 17	Plot of amplitude ratio data from Table 3.	66
Fig. 18	Plot of amplitude ratio data from Table 4.	67
Fig. 19	Plot of phase data from Table 1.	68 ✓

		<u>Page No.</u>
Fig. 20	Plot of phase data from Table 2	69
Fig. 21	Plot of phase data from Table 3	70
Fig. 22	Plot of phase data from Table 4	71
Table 5	Summary of fitted describing functions	72
Table 6	Attitude error and pilot response power spectrum for fixed base session, $\omega_{nbd} = 5$ rad/sec.	73
Table 7	Attitude error and pilot response power spectrum for fixed base session, $\omega_{nbd} = 7$ rad/sec	74
Table 8	Attitude error and pilot response power spectrum for moving base session, $\omega_{nbd} = 7$ rad/sec	75
Table 9	Attitude error and pilot response power spectrum for moving base session, $\omega_{nbd} = 5$ rad/sec	76
Fig. 23	Plot of control stick power from Table 6	77
Fig. 24	Plot of control stick power from Table 7	78
Fig. 25	Plot of the RMS ratio $\sqrt{\frac{\sigma_y^2}{\sigma_x^2}}$ versus bending mode amplitude for fixed base plus simulated dynamics experiments.	79
Fig. 26	Individual tracking run $\sqrt{\frac{\sigma_y^2}{\sigma_x^2}}$ scores versus bending mode amplitude for each subject under fixed base, $\omega_{nbd} = 7$ rad/sec conditions	80
Table 10	Analysis of variance results for Fig. 26	81
Fig. 27	Plot of $\sqrt{\frac{\sigma_y^2}{\sigma_x^2}}$ results versus bending mode amplitude for each type of simulation at $\omega_{nbd} = 7$ rad/sec	82

Fig. 28	Plot of averaged $\sqrt{\bar{e}^2/\bar{d}^2}$ results versus bending mode amplitude for each type of simulation at $\omega_{nbd} = 5$ rad/sec	83
Fig. 29	Comparison of $\sqrt{\bar{e}^2/\bar{d}^2}$ results for $\omega_{nbd} = 5$ and 7 rad/sec during fixed base conditions	84
Fig. 30	Comparison of $\sqrt{\bar{e}^2/\bar{d}^2}$ results for $\omega_{nbd} = 5$ and 7 rad/sec during moving base conditions	85
Fig. 31	Comparison of $\sqrt{\bar{e}^2/\bar{d}^2}$ results for $\omega_{nbd} = 5$ and 7 rad/sec during fixed base plus simulator dynamics conditions	86
Fig. 32	Plot of $\sqrt{\bar{e}^2/\bar{d}^2}$ results versus bending mode amplitude for conditions of low RMS disturbance signal	87
Fig. 33	Plot of $\sqrt{\bar{e}^2/\bar{d}^2}$ results versus bending mode amplitude for condition of low RMS disturbance signal	88
Fig. 34	Comparison of $\sqrt{\bar{e}^2/\bar{d}^2}$ results for the two disturbance signals with $\omega_{nbd} = 7$ rad/sec	89
Fig. 35	Comparison of $\sqrt{\bar{e}^2/\bar{d}^2}$ results for the two disturbance signals with $\omega_{nbd} = 5$ rad/sec	90
Fig. 36	Effective dynamics as seen by pilot for simplified versions of two proposed vehicle augmentation and control stick filter schemes	91
Table 11	Summary of results comparing the two proposed vehicle augmentation and control stick filter schemes	92
Fig. A1	Root locus 1	93
Fig. A2	Root locus 2	94

LIST OF SYMBOLS

$F_\alpha$ $F_\beta$ $F_\phi$	Partial derivatives of the force on the missile with respect to $\alpha$ , $\beta$ , $\phi$ , respectively.
$M_\alpha$ $M_\beta$	Partial derivatives of the moment on the missile with respect to $\alpha$ and $\beta$ respectively.
$\alpha$	Pitch angle of attack.
$\beta$	Engine gimbal angle.
$\phi_{tot}$	Total pitch attitude angle with respect to nominal trajectory.
$\phi_{rb}$	Part of $\phi_{tot}$ due to the rigid body mode.
$\phi_{bd}$	Part of $\phi_{tot}$ due to the flexible body mode.
$V$	Nominal vehicle velocity.
$\omega_{nrb}$	Natural frequency of the rigid body mode.
$\omega_{nbd} = \omega_p$	Natural frequency of the bending mode.
$\omega_z = 3\omega_{nbd}$	Location of the zeroes associated with the first bending mode.
$K_{11}$ $K_{21}$ $K_{31}$	Constants associated with the bending mode.
$K$	Constant proportional to the amplitude of the bending mode.
$K_{rl}$	Root locus gain.

n	Generalized coordinate associated with the first bending mode.
$q_i$	ith zero in transfer function.
$p_i$	ith pole in transfer function.
p	LaPlace operator.
ISE	Integral squared error.
d(t)	Disturbance signal into the control loop.
e(t)	Displayed attitude error.
s(t)	Operator's response.
o(t)	Output of simulated missile dynamics.
$\sqrt{\frac{\int_0^T [e(t)]^2 dt}{\int_0^T [d(t)]^2 dt}} = \sqrt{\frac{\sigma_e^2}{\sigma_d^2}}$	RMS ratio of the attitude error to disturbance signal for one tracking run.
$\sqrt{\frac{\sigma_e}{\sigma_d}}$	The same ratio averaged over several tracking runs.
$\sqrt{\frac{\int_0^T [s(t)]^2 dt}{\int_0^T [e(t)]^2 dt}} = \sqrt{\frac{\sigma_s^2}{\sigma_e^2}}$	RMS ratio of the pilot response to attitude error for one tracking run.
$\sqrt{\frac{\sigma_s}{\sigma_e}}$	The same ratio averaged over several tracking runs.
nom.	The amplitude of the bending mode at the proposed location of the Saturn V attitude gyro.

## CHAPTER I

### INTRODUCTION

Several relatively recent studies have been conducted to determine the feasibility of using a pilot to control the attitude and trajectory of large flexible boosters during the launch into orbit. Along with other problems, these investigations considered the ability of the pilot to effectively control the unstable rigid body mode without exciting the relatively low frequency and highly sensitive bending mode beyond structural or attitude limitations.

Hardy, et al, simulated the rigid and flexible body dynamics of the Saturn V booster and report that the visual and vestibular cues from flexible motions did not create serious problems.<sup>1</sup> However, they obtained these results using a second order low pass filter to attenuate the high frequency components of the control stick output.

In a theoretical study, Teper and Jex agree that it would be possible for the pilot to directly control the missile, but recommend, among other things, replacing the second order stick filter with a single integration.<sup>7</sup>

In either case, stick filters reduce the bending mode effect at the cost of additional phase lag in series with an already difficult set of missile dynamics.

The objective of this thesis is to study more comprehensively the effect of a superimposed bending mode on the pilot's ability to control the single axis attitude of a missile with unstable rigid body dynamics. Hopefully, in spite of the restrictions to a particular set of rigid body dynamics, the results will be applicable to other missiles and large aircraft with significant flexible modes.

The importance of the bending mode depends on many control system parameters and pilot characteristics. However, the relative natural frequencies of the two modes, the amplitude of the bending mode, and the type of simulation, fixed or moving base, were considered the most important, and attention was directed primarily at these factors.

In general, the interaction between two modes in a feedback control system increases as the separation between the natural frequencies decreases. In this situation, there will be a direct relation between the degree of excitation of the bending mode and the frequency content of the control stick signal. In turn, this frequency content will be determined partly by the difficulty of the rigid body control task assigned to the pilot.

The simulated system dynamics included the dominant inverted pendulum rigid body mode of the Saturn V at peak dynamic pressure  $\omega_{nr}^2 = .15$ , and the first bending mode. Bending mode frequencies of  $\omega_{nb}^2 = 49$  (rad/sec)<sup>2</sup> and 25 (rad/sec)<sup>2</sup> were studied. The first bending mode natural frequency of the Saturn V at maximum dynamic pressure equals approximately 49 (rad/sec)<sup>2</sup>. A value significantly closer

to the pilot control frequencies chosen for the second frequency.

For a given natural frequency, the flexible mode acceleration sensed by the pilot is proportional to the mode amplitude. An amplitude approximately equal to that sensed at the proposed attitude gyro station for the Saturn V was taken as a nominal value. Three other amplitudes, (0, .33 nom., and 2.0 nom.), were studied in the fixed base experiments. A wider range, (0 to 4.0 nom), were used for the moving base work. The decrease in effective pilot control fixed the upper limit on the amplitude, and the onset of significant bending mode effects determined the lower.

The pilot senses the existence of the bending mode by visual and vestibular cues. In order to assess the relative importance of these two inputs, the experiments were performed both fixed and moving base using a single axis of rotation.

Fig. 1 contains a block diagram showing the position of the pilot, booster, displays, disturbance signal, and possible compensations in the signal axis control loop. Fig. 2 shows the components used for this investigation.

For the purposes of this study, display and stick filters were not used except for a brief comparison of two suggested stick filters. The control stick filter was eliminated to find the deterioration of uncompensated pilot performance with increasing bending mode amplitude. From comparisons of the resulting increases in attitude error and structural loadings with attitude specifications and structural limitations, bending

mode amplitudes requiring the additional complexities of control stick filters may be determined.

Rigid body rate compensation was added after preliminary experiments indicated the combination of uncompensated dynamics, noise signal, and bending mode created a very difficult control problem. No bending mode rate information was included in the rate signal. Perfect filtering of the flexible portion of the rate signal was assumed in order to study only direct control stick excitation of the bending mode.

A random noise disturbance signal summed with the simulated dynamics output produced the moving base drive signal to the simulator and the fixed base error signal. The random noise signal replaced the wind spike disturbance of Ref. 1 to allow pilot transfer function computations. The noise signal entered as an attitude angle and not an acceleration into the dynamics, once again, to restrict direct bending mode excitation to the control stick output.

The RMS value of the disturbance signal was chosen so that typical RMS attitude errors ranged from one to three degrees. These errors could be controlled with the maximum control torque of  $4.4^\circ/\text{sec}^2$ . This value was inadvertently made 15% higher than that recommended in Ref. 1.

The disturbance consisted of a white Gaussian signal shaped by two first order filters with break frequencies at 1 rad/sec. Two factors determined the frequency content of the signal. First, the noise signal had to contain sufficient

high frequency power to permit computation of a transfer function valid to .8 cps. Secondly, the signal could not vary so rapidly that the subject was unable to control the rigid body portion of the error signal.

Bending mode influence on pilot performance was measured by error to disturbance and pilot control stick output to error signal ratios, and by pilot transfer functions.

The experimental part of the thesis consisted of both fixed and moving base studies of variations in bending mode amplitude and natural frequency, and extended fixed base studies including simulator dynamics, disturbance signals with lower RMS values, and stick filters.

## CHAPTER II

## SIMULATION AND EQUIPMENT

This chapter describes the simulated missile dynamics, and the equipment needed to instrument the control loop of Fig. 2.

The equations of motion and parameter values describing the pitch axis dynamics of the Saturn V booster at maximum dynamic pressure were taken from Ref. 1. The linearized rigid body equations for small perturbations from the nominal trajectory are:

$$\ddot{x} = -F_{\alpha}\alpha - F_{\phi}\phi_{rb} - F_{\beta}\beta \quad (2.1)$$

$$\ddot{\phi}_{rb} = M_{\alpha}\alpha - M_{\beta}\beta \quad (2.2)$$

$$\alpha = \phi_{rb} + \frac{57.3}{V} \dot{x} \quad (2.3)$$

In Appendix 1, these equations are reduced to the following relation between  $\phi_{rb}$  and  $\beta$ :

$$\frac{\phi_{rb}}{\beta} = -M_{\beta} \frac{(p + \frac{M_{\alpha}}{M_{\beta}} \frac{F_{\beta}}{V} 57.3 + F_{\alpha} \frac{57.3}{V})}{(p^3 + \frac{57.3}{V} F_{\alpha} p^2 - M_{\alpha} p + \frac{57.3}{V} M_{\alpha} F_{\alpha})} \quad (2.4)$$

After replacing the parameters with their values at maximum dynamic pressure and factoring:

$$\frac{\phi_{rb}}{\beta} = -1.15 \frac{(p + .0197)}{(p - .34)(p + .40)(p - .0425)} \quad (2.5)$$

This expression is simplified in Appendix 1 to:

$$\frac{\phi_{rb}}{\beta} \approx - \frac{7.67(.15)}{(p^2 - .15)} \quad (2.6)$$

Finally, when the rigid body rate compensation recommended in Ref. 1 is added, results in Appendix 1 show:

$$\frac{\phi_{rb}}{\beta} \approx - \frac{7.67(.15)}{(p + 1.00)(p - .15)} \quad (2.7)$$

The elastic body mode may be represented by:

$$\frac{\phi_{bd}}{\beta} = \frac{K_{31}K_{21}(p^2 + \frac{K_{11}}{K_{21}})}{(p^2 + 2\xi\omega_{nbd}p + \omega_{nbd}^2)} \quad (2.8)$$

From Appendix 1, after certain assumptions and parameter value substitutions, the equation becomes:

$$\frac{\phi_{bd}}{\beta} = \frac{K(p^2 + 21^2)}{(p^2 + .01(7)p + 7^2)} \quad \text{for } \omega_{nbd} = 7 \text{ rad/sec} \quad (2.9)$$

$$\frac{\phi_{bd}}{\beta} = \frac{K(p^2 + 15^2)}{(p^2 + .01(5)p + 5^2)} \quad \text{for } \omega_{nbd} = 5 \text{ rad/sec} \quad (2.10)$$

The total expression for  $\phi_{tot}/\beta$  in terms of K, a number proportional to the bending mode amplitude, and  $\omega_{nbd}$ , the natural frequency, becomes:

$$\frac{\phi_{tot}}{\beta} = \frac{-1.15(p^2 + .01\omega_{nbd}p + \omega_{nbd}^2) + K(p^2 + (3\omega_{nbd})^2)(p - .15)(p + 1.00)}{(p - .15)(p + 1.00)(p^2 + .01\omega_{nbd}p + \omega_{nbd}^2)} \quad (2.11)$$

The root locus technique is used in Appendix 1 to factor the numerator of (2.11) for the two values of  $\omega_{nbd}$  (5 and 7 rad/sec) and four values of K (.0022, .0066, .0132, .0264).

The results are listed below:

$$\omega_{nbd} = 7 \text{ rad/sec,}$$

$$K = .0022 \quad \frac{\phi_{tot}}{\beta} \approx \frac{.0022(p + 19)(p - 18.6)(p^2 + 10^2)}{(p - .15)(p + 1.00)(p^2 + .01(7)p + 7^2)} \quad (2.12)$$

$$K = .0066 \quad \frac{\phi_{tot}}{\beta} \approx \frac{.0066(p + 7.1)(p - 6.5)(p^2 + (15.9)^2)}{(p - .15)(p + 1.00)(p^2 + .01(7)p + 7^2)} \quad (2.13)$$

= (nom.)

$$K = .0132 \quad \frac{\phi_{tot}}{\beta} \approx \frac{.0132(p + 4.5)(p - 3.8)(p^2 + (18.6)^2)}{(p - .15)(p + 1.00)(p^2 + .01(7)p + 7^2)} \quad (2.14)$$

$$K = .0264 \quad \frac{\phi_{tot}}{\beta} \approx \frac{.0264(p + 3.2)(p - 2.4)(p^2 + (19.5)^2)}{(p - .15)(p + 1.00)(p^2 + .01(7)p + 7^2)} \quad (2.15)$$

$$\omega_{nbd} = 5 \text{ rad/sec}$$

$$K = .0022 \quad \frac{\phi_{tot}}{\beta} \approx \frac{.0022(p + 22.7)(p - 22.7)(p^2 + (5.8)^2)}{(p - .15)(p + 1.00)(p^2 + .01(5)p + 5^2)} \quad (2.16)$$

$$K = .0066 \quad \frac{\phi_{tot}}{\beta} \approx \frac{.0066(p + 9.4)(p - 8.8)(p^2 + (8.8)^2)}{(p - .15)(p + 1.00)(p^2 + (.01)5 p + 5^2)} \quad (2.17)$$

$$K = .0132 \quad \frac{\phi_{tot}}{\beta} \approx \frac{.0132(p + 5)(p - 4.3)(p^2 + (11.5)^2)}{(p - .15)(p + 1.00)(p^2 + (.01)5 p + 5^2)} \quad (2.18)$$

$$K = .0264 \quad \frac{\phi_{tot}}{\beta} \approx \frac{.0264(p + 3.3)(p - 2.6)(p^2 + (13.2)^2)}{(p - .15)(p + 1.00)(p^2 + (.01)5 p + 5^2)} \quad (2.19)$$

Figs. 3 and 4 show the analog computer program for the simulation of these missile dynamics. An EAI TR-48 analog computer was used for the fixed base investigations and Philbrick amplifiers for the moving base experiments.

For the case of the experiments concerning the stick filter proposed in Ref. 2, the dynamics associated with rigid body change. Teper and Jex recommend, in addition to the single integration stick filter, feeding back position as well as rate information.

Appendix 1 shows that with these modifications and certain simplifications the effective rigid body dynamics become:

$$\frac{\phi_{rb}}{\beta} = \frac{- .85(4)}{p^2 + 2(.56)2 p + 2^2} \quad (2.20)$$

With this change in rigid body dynamics the relation between  $\phi_{tot}$  and  $\beta$  becomes:

$$\frac{\phi_{tot}}{\beta} = \frac{-3.4(p^2 + .01(7)p + 7^2) + .0066(p^2 + 2(.56)2p + 2^2)(p^2 + 21^2)}{(p^2 + 2(.56)2p + 2^2)(p^2 + (.01)7p + 7^2)} \quad (2.21)$$

The root locus technique is applied to factor the numerator and the results appear below for  $K = .0066$  and  $\omega_{nbd} = 7$  rad/sec.

$$\frac{\phi_{\text{tot}}}{\beta} = \frac{.0066(p + 11)(p + 15.5)(p^2 + (10.5)^2)}{(p^2 + 2(.56)2p + 2^2)(p^2 + (.01)7p + 7^2)} \quad (2.22)$$

The modified analog computer program for these equations appears in Fig. 5.

Fig. 6 contains the analog computer program required to unbias, amplify, and filter the random noise signal. The signal on the tape recorder had a frequency spectrum flat to 1000 cps.

A motion simulator capable of rotation about two axes was used for the moving base experiments (see Fig. 7). Because of superior roll frequency response, the experiments were performed about the roll and not pitch axis. The frequency response of the simulator with subject was measured and found to be second order with a natural frequency of 1.6 cps and a damping ratio,  $\xi$ , equal to .4. The phase shift at .8 cps was  $30^\circ$  and  $55^\circ$  at 1.2 cps. A dead-zone of approximately  $1/3^\circ$  existed.

The characteristics of the control sticks for the fixed and moving base experiments appear in Fig. 8. The fixed base control stick was restrained by a stronger spring.

Attitude error, fixed base, and cab position, moving base, was the only information displayed to the subject. In both cases, the error angle was represented on an oscilloscope

by the horizontal distance from the center of the screen to a generated vertical line. The scope sensitivity was 1 cm/deg for fixed base work and .6 cm/deg for moving base experiments.

Four signals, disturbance, attitude error, stick output, and simulated missile dynamics output were recorded on strip chart recorders and a four channel F-M tape recorder, (see Fig. 9).

Figs. 10 and 11 show the subjects' position, display, and control stick for the fixed and moving base investigations respectively.

## CHAPTER III

## PROCEDURE

Three students served as subjects in the experiments. The subjects were screened by testing their ability to control unstable dynamics in a compensatory tracking task and to balance on one foot without visual cues.

After selection, the subjects practiced controlling the Saturn V dynamics until no further improvement in performance could be detected.

Typically, sessions lasted two hours and included twenty to twenty-five tracking runs of 90 or 120 seconds separated by three minute rest periods.

During a session, only the bending mode amplitude changed. Usually, the session was divided into six runs at each of four amplitudes. The bending mode amplitude increased as the session progressed.

Before each session, the subjects were informed of the bending mode natural frequency. In addition, they were told of changes in bending mode amplitude.

The subjects were instructed to use the control stick as necessary to minimize the displayed error until the distraction of bending mode oscillations forced a reduction of control efforts. The subjects learned fairly quickly by trial and error how much control to use at each bending mode amplitude.

The chart below shows the content and sequence of the sessions and the participating subject.

SIMULATION DETAILS	SUBJECT	BENDING MODE NATURAL FREQUENCY AND AMPLITUDE RANGE			
A FIXED BASE CONDITIONS	S.K.	#1, $\omega_{nbd}=7$ K=0 TO 2(NOM)	#4, $\omega_{nbd}=7$ K=0 TO 2(NOM)	#7, $\omega_{nbd}=5$ K=0 TO 2(NOM)	#8, $\omega_{nbd}=5$ K=0 TO 2(NOM)
	R.J.	#3, $\omega_{nbd}=7$ K=0 TO 2(NOM)	#5, $\omega_{nbd}=7$ K=0 TO 2(NOM)	#9, $\omega_{nbd}=5$ K=0 TO 2(NOM)	#10, $\omega_{nbd}=5$ K=0 TO 2(NOM)
	E.S.	#2, $\omega_{nbd}=7$ K=0 TO 2(NOM)	#6, $\omega_{nbd}=7$ K=0 TO 2(NOM)	—	—
B MOVING BASE CONDITIONS	R.J.	#12, $\omega_{nbd}=7$ K=0 TO 2(NOM)	#16, $\omega_{nbd}=7$ K=0 TO 4(NOM)	#14, $\omega_{nbd}=5$ K=0 TO 3(NOM)	#15, $\omega_{nbd}=5$ K=0 TO 4(NOM)
	E.S.	#11, $\omega_{nbd}=7$ K=0 TO 2(NOM)	#13, $\omega_{nbd}=7$ K=0 TO 4(NOM)	—	—
C FIXED BASE & SIMULATOR DYN. MOVING BASE STICK & DISPLAY	R.J.	#17, $\omega_{nbd}=7$ K=0 TO 4(NOM)	#19, $\omega_{nbd}=7$ K=0 TO 4(NOM)	#18, $\omega_{nbd}=5$ K=0 TO 4(NOM)	#20, $\omega_{nbd}=5$ K=0 TO 4(NOM)
D FIXED BASE CONDITIONS EXCEPT LOW RMS DISTURBANCE	R.J.	#21, $\omega_{nbd}=7$ K=0 TO 2(NOM)	#23, $\omega_{nbd}=7$ K=0 TO 2(NOM)	#22, $\omega_{nbd}=5$ K=0 TO 2(NOM)	#24, $\omega_{nbd}=5$ K=0 TO 2(NOM)
E FIXED BASE LOW RMS DISTURBANCE VEHICLE AUGMENTATION & STICK FILTER OF HARDY, ET AL.	R.J.	#25, $\omega_{nbd}=7$ K=NOM 10 TRACKING RUNS	#26, $\omega_{nbd}=7$ K=NOM 10 TRACKING RUNS	—	—
F FIXED BASE LOW RMS DISTURBANCE VEHICLE AUGMENTATION & STICK FILTER APPROXIMATION TO TEPER & JEX	R.J.	#27, $\omega_{nbd}=7$ K=NOM 10 TRACKING RUNS	#28, $\omega_{nbd}=7$ K=NOM 10 TRACKING RUNS	—	—
G FIXED BASE CONDITIONS - BENDING MODE AMPLITUDE UNKNOWN TO SUBJECT	R.J.	#29, $\omega_{nbd}=7$ K=133 NOM 10 TRACKING RUNS	—	—	—

The experiments in Series C were conducted to find what part of the difference between fixed and moving base results should be attributed to the combination of simulator dynamics, decreased display sensitivity, and lightly restrained control stick.

The interaction between disturbance signal amplitude and performance deterioration with increasing bending mode amplitude was studied in Series D.

Series E and F reflect curiosity about the effect of essentially changing the dynamics the pilot must control from fourth to either fifth or sixth order by the addition of a stick filter.

To confirm that deterioration in performance with increasing bending mode amplitude did not occur because of the order of presentation or knowledge of amplitude, a subject, without this information, was tested in Series G.

Fatigue was checked as a possible factor by testing the subjects' ability to control the rigid body mode alone at various times during the two hour sessions.

Integral square error values of the noise, error, and stick output signals were calculated by amplifying, squaring, attenuating and integrating these signals for each run. Fig. 12 contains the analog computer patching program that performed these operations.

These scores, pilot transfer functions, and strip chart recordings provided the means to analyze the effect of variations in dynamics and experimental conditions.

The error to disturbance ratio,  $\sqrt{e^2/d^2}$  measured the pilot's ability to control the attitude of the simulated missile.

The control output to error ratio,  $\sqrt{z^2/d^2}$  and pilot transfer functions show more directly the results of changing conditions on the pilot.

This second ratio represents an average gain for the pilot for the run, but ignores the well-known dynamics associated with the human operator.

The pilot transfer functions were computed by a spectral analysis method described in Appendix 2.

The approximate levels of accelerations due to bending mode oscillations were determined by analysis of the individual strip chart recordings. These recordings also show clearly changes in pilot control actions as a function of bending more amplitude.

## CHAPTER IV

## DISCUSSION OF RESULTS

The effect of variations in bending mode parameters and simulation conditions will be discussed from two standpoints:

1. Changes in pilot control characteristics.
2. Changes in closed loop attitude error performance.

Strip chart recordings of the displayed attitude error and control stick movement are presented in Figs. 13 and 14. These are taken from a fixed base session with  $\omega_{nbd} = 7$  rad/sec. These recordings show qualitatively the reduction of effective pilot control and the increase in attitude error as the bending mode amplitude increases.

With the bending mode removed entirely, the pilot used all available control power and behaved very non-linearly. In this case, only the amount of control power as set by the Saturn V recommendations of Ref. 1 restricted the pilot, and the control stick output contained a significant amount of high frequency power. A revision in pilot control strategy became necessary with non-zero bending mode amplitudes. If the subject failed to restrain

his control action, intolerable bending mode oscillations developed at even the lowest amplitude (1/3 nom.) under study. In the process of attempting to alleviate this problem, the subject began to lose effective control of the rigid body portion of the attitude error.

To analyze these effects more quantitatively, several criteria were employed. Pilot describing functions were measured for four sessions by a power spectral technique explained in detail in Appendix B and associated references.<sup>5,6</sup> Power spectral estimates of the attitude error and control stick signals are available from the describing function computation. In addition, RMS ratios of the control stick to the attitude error signal,  $\sqrt{s^2/e^2}$ , and the attitude error to disturbance signal,  $\sqrt{e^2/d^2}$ , were measured for the individual tracking runs.

The describing function was calculated by the following formula:

$$Y_p(j\omega) = \frac{\phi_{13}(\omega)}{\phi_{12}(\omega)} \quad (4.1)$$

where:

$\phi_{13}(\omega)$  = the cross power spectral estimate between the disturbance signal and the control stick signal

$\phi_{12}(\omega)$  = the cross power spectral estimate between the disturbance signal and the displayed error signal.

The degree to which the describing function accounted for the pilot's behavior was measured by the correlation coefficient:

$$\rho^2 = \frac{|\Phi_{13}(\omega)|^2}{\Phi_{11}(\omega) \Phi_{33}(\omega)} \quad (4.2)$$

where:

$\Phi_{11}(\omega)$  = the power spectrum of the disturbance signal

$\Phi_{33}(\omega)$  = the power spectrum of the control stick signal

The value of  $\rho^2$  should be near unity if the describing function accounts for most of the operator's characteristics.

The describing function data is presented in Tables 1 through 4 and plotted in Figures 15 through 22. The amplitude data and fitted amplitude ratios appear in the first four figures. The phase data are shown in the last four. Pertinent information about the associated experimental condition is listed in the Tables.

It should be noted that the correlation coefficients are not close to unity above 3 rad/sec for the fixed base experiments and 2 rad/sec for the moving base work.

The recorded disturbance signal contained occasional spikes from an extraneous source. These spikes showed up as an uncorrelated wide-band signal superimposed on the spectrum of the disturbance. On the average, the wide-band spectrum amplitude reached 1/10 of the disturbance signal

power spectrum at 2.7 rad/sec fixed base, and at 1.8 rad/sec moving base.

Above these frequencies, the reliability of the data drops sharply because only a fraction of the disturbance signal is uncontaminated. However, the form of the amplitude and phase data remains reasonable to 3.6 rad/sec. With these factors in mind, the describing function results are retained up to this frequency.

The describing functions are summarized in Table 5.

The important results are:

1. The level of pilot gain decreases as the bending mode amplitude increases.
2. The phase lead generated by the pilot decreases with increasing bending mode amplitude.
3. The subjects' gain was significantly lower during the moving base tests than in the fixed base experiments.

The lowering of subject gain reflects his attempts to minimize bending mode excitations.

The decrease in phase lead as the bending mode amplitude increases seems to be best accounted for by a larger dead-time delay in the pilot describing function. There is some shifting of the pole-zero combination, but this is not a major factor.

The distinct reduction of subject moving base gain compared with fixed base results was unexpected. Simulation and scaling factors were carefully checked for errors that might explain the effect.

The power spectral estimates of the error signal presented in Tables 6 through 9 show that the reduced moving base gain occurs because of increased error rather than lower control stick power.

A series of fixed base experiments including the second order dynamics and dead-zone associated with the motion simulator plus the moving base control stick and display will be discussed in more detail later. However, these experiments did not indicate that the increased error could be attributed entirely to these factors. It should be pointed out, though, that not all the motion simulator non-linearities, such as stiction and backlash, were considered. The effect of these factors cannot be discounted because typical simulator movements were within the range of  $\pm 5^\circ$ .

Apart from this, the increased errors may be attributed to subject uncertainty about the location of the vertical during the moving base simulation. The subject's vestibular system may provide orientation information that is in error by a degree or two. Furthermore, the scale on the moving base display was less sensitive and the grid was not as well defined as the fixed base display.

In spite of the reduced gain, the subject was able to generate the same amount if not more phase lead. For these reasons, the best explanation seems to involve neglected simulation non-linearities, a less sensitive

display, and perhaps vestibular confusion and insensitivity concerning very small angular deflections about the vertical.

Tables 6 through 9 include the power spectral estimates of the error and control stick for the four sessions where describing functions were computed.

The control stick power from Tables 7 and 8 has been plotted in Figures 23 and 24. These power spectral estimates show:

1. In general pilot control power at the primary rigid body control frequencies of .45 to 1.8 rad/sec decreases with increasing bending mode amplitudes. There are exceptions to this statement, however, considering the increases in rigid body error power at these frequencies, effective pilot control has certainly decreased. The same general effect appears on the amplitude plots for the describing function. In this case there is no consideration of linear correlation.

2. In certain cases, there has been an attempt to track the higher frequency bending mode error as indicated by secondary peaks a little below the bending mode natural frequency.

3. Control stick power drops drastically with increasing bending mode amplitude at and above the natural frequency.

4. The subjects were remarkably adaptive in their attempts to avoid bending mode excitation by elimination

of the high frequency components from their control stick action.

The reduced gain versus increased bending mode amplitude is shown by a slightly different criterion in Fig. 25. The RMS ratio of control stick signal to error signal,  $\sqrt{s^2/e^2}$ , is plotted versus bending mode amplitude for the set of fixed base experiments including simulator dynamics. This ratio represents a pseudo-gain for the subject that ignores dynamics and linear correlation. Once again, pilot gain is inversely related to bending mode amplitude. The decreasing gain consists of both in increasing RMS error and decreasing RMS control power.

The ratio of the RMS value of the error to disturbance signal,  $\sqrt{e^2/d^2}$  measures the effect of variations in pilot control strategy on closed loop performance.

Before discussing the main body of  $\sqrt{e^2/d^2}$  results, several tests for spurious variables will be described. Three subjects were used for the fixed base experiments with the bending mode natural frequency,  $\omega_{\text{nbđ}} = 7$  rad/sec. In order to check intersubject differences an analysis of variance was performed on the results of this series of experiments. Intersession and intersubject variances were compared for each of the four amplitudes. Fig. 26 presents the individual tracking run scores for the two sessions under study for each of the subjects. Table 10 shows the results of the analysis of variance.

The intersubject interaction was significant at the .05 level for only one amplitude  $2x(\text{nom.})$ . On this basis intersubject interactions were ignored.

In order to test the importance of subject knowledge of the bending mode amplitude and the fixed order of bending mode amplitude variations, ten tracking runs were taken at an amplitude, 1.33 nom., unknown to the subject. The experimental conditions were: fixed base simulation, and  $\omega_n = 7$  rad/sec. The average,  $\sqrt{e^2/d^2}$  score was .84 compared with an expected .70 based on results that will appear in Fig. 27. If such a limited amount of data is significant at all, it would indicate that subject performance at a given amplitude would not improve if the amplitude was varied randomly with no information being given to the subject.

On several occasions,  $\sqrt{e^2/d^2}$  scores for the condition of no superimposed bending mode were taken towards the end of a session. No increase in these scores over the ones at the start of the session was noted indicating no fatigue effects.

The  $\sqrt{e^2/d^2}$  ratio is plotted against the four  $\omega_{\text{nbd}} = 7$  rad/sec bending mode amplitudes for the three types of simulation, fixed base, moving base, and fixed base plus simulator dynamics in Fig. 27. The scores plotted for each amplitude and type of simulation represents the average of all the individual tracking runs for the specific condition.

Both moving and fixed base experiments were performed in an attempt to find the relative importance of vestibular and visual cues. The fixed base experiments with the second order dynamics and dead-zone of the motion simulator plus moving base display and control stick were conducted to find the significance of these factors.

The results show that:

1. The  $\sqrt{e^2/a^2}$  ratio increases significantly with increasing bending mode amplitude.

2. The attitude error is much larger for moving base experiments compared with the fixed base.

3. This difference cannot be completely accounted for by any conditions tested in the fixed base plus simulated dynamics series.

4. The attitude error increases less rapidly for the moving base and fixed base plus simulated dynamics than for the fixed base experiments.

The first result reflects decreased subject gain and phase lead generation.

The second has been discussed earlier in the chapter.

Since the rate of attitude error increase is similar for the moving base and fixed base plus simulator dynamics, the difference between the fixed and moving base rates cannot be necessarily attributed to vestibular effects.

Unfortunately, the dead-zone associated with the motion simulator suppresses bending mode oscillations, and makes fixed and moving base comparisons difficult.

This emphasizes the fact that moving and fixed base differences can be the result of vestibular effects or simulator characteristics. Furthermore, the simulator dynamics and non-linearities must be located at a very bad place, between the actual position and the displayed position, in this control loop. For this reason, the fixed base results are probably more realistic and reliable.

The same results are plotted in Fig. 28 for the bending mode of natural frequency  $\omega_n = 5$  rad/sec. The general trends are very similar. The  $\sqrt{e^2/d^2}$  ratio has been plotted versus amplitude and not effective acceleration. For the same bending mode amplitude, the effective acceleration for  $\omega_{nbd} = 5$  rad/sec is only 1/2 of the acceleration for the case of  $\omega_{nbd} = 7$  rad/sec.

Comparisons of the  $\sqrt{e^2/d^2}$  ratio for  $\omega_{nbd} = 5$  and 7 rad/sec are plotted for each type of simulation in Figures 29 through 31 versus amplitude and not effective acceleration. The  $\sqrt{e^2/d^2}$  ratio increased more rapidly for  $\omega_n = 5$  during fixed base simulation and for  $\omega_n = 7$  during fixed base plus simulator dynamics. On the other hand, there was little difference during the moving base simulation. The only certain conclusion is that one-half the acceleration at  $\omega_{nbd} = 5$  rad/sec compared with

$\omega_{\text{nb}} = 7$  rad/sec caused approximately the same performance deterioration.

The results from the fixed base experiments using a disturbance signal with one-half the RMS value of the previous experiments appear in Figures 32 through 35.

The averaged  $\sqrt{e^2/d^2}$  scores for the two sessions at both  $\omega_{\text{nb}} = 5$  and 7 rad/sec are presented in Fig. 32. Consistent with the earlier fixed base results, the attitude error for a given amplitude is greater for  $\omega_{\text{nb}} = 5$  rad/sec.

Fig. 33 contains the  $\sqrt{3e^2/e^2}$  results for the same conditions. Note, that at each amplitude, the subject gain is lower for  $\omega_{\text{nb}} = 5$  rad/sec curve and the attitude error is greater. This same correlation between gain and error holds at each amplitude for the fixed base plus simulated dynamics experiments except that the gain is lower and attitude error greater for  $\omega_{\text{nb}} = 7$  rad/sec, see Fig. 25, 27, and 28.

With this correlation in mind, the interaction between the RMS value of the disturbance signal and the rate of  $\sqrt{e^2/d^2}$  increases with respect to bending mode amplitude will be examined. Comparisons of the attitude error performance for the two disturbance signals at each bending mode natural frequency appears in Figs. 34 and 35.

Somewhat surprisingly, for each non-zero bending mode amplitude and both frequencies, the subjects'  $\sqrt{e^2/d^2}$  score was better for the high RMS disturbance signal. In

addition, for the one high RMS fixed base session where the  $\sqrt{s^2/e^2}$  ratio was measured, the subject operates with a higher gain for the low RMS disturbance signal. This result is not consistent with the previous high gain ratio-low error ratio correlation just discussed.

The final series of experiments studied two vehicle augmentation and control stick filtering schemes. Both approaches have been simplified, and the simulated dynamics are only first approximations to the actual control systems.

For all previous experiments, the augmented missile dynamics have been similar to those proposed by Hardy, et al, in Ref. 1. To approximate the entire system recommended there, a second order stick filter was added in series with these dynamics. The effective dynamics as seen by the subject appear in Fig. 36a.

The simplification of the missile augmentation proposed by Teper and Jex in Ref. 7 has been discussed in Appendix A. The single integration-gain stick filter was placed in series with this set of simplified dynamics to form the complete system, as shown in Fig. 36b.

The bending mode amplitude was fixed at the nominal value and the natural frequency at 7 rad/sec for all experiments in this series.

Twenty tracking runs divided between two sessions were taken for each system.

Before discussing the results, the choice of one parameter must be explained. There was some uncertainty about the correct choice of maximum control torque for the single integration system. Up to the present, the maximum torque has been  $1.15^\circ / \text{sec}^2 / \beta$  with  $\beta_{\text{max}} = 3.87^\circ$ . Preliminary experiments with both systems indicated that the second order filter removed about 10% of the pilot response signal, and the single integration-attenuation filter output was 1/3 of the pilot's response. For this reason, the maximum control was increased by a factor of three for the latter system.

For these experiments, the  $\sqrt{s^2/a^2}$  ratio was measured for both the control stick output and the stick filter output signal. As usual, the attitude control was measured by the  $\sqrt{e^2/a^2}$  ratio.

The results are summarized in Table 11 and show that:

1. The average  $\sqrt{e^2/a^2}$  ratio for the single integration-stabilized dynamics version was .88, compared with 1.20 for the second order-rate augmented dynamics system
2. Both systems reduced bending mode excitation to an occasional oscillation or two at an amplitude of less than one-half degree.
3. As mentioned earlier, the single integration filter removed a much greater portion of the operator's response than the second order filter.

4. The effective pilot gain, as measured after the filter, is higher for the case of stable rigid poles and single integration stick filter.

Because of this last reason, the improved performance with the approximation to Jex and Teper's proposal may be due to the arbitrarily increased control torque. However, the complete stabilization of the rigid poles seems like a very reasonable suggestion, and should contribute to improved performance. On the other hand, the single integration-attenuation filter suppresses a large percentage of the operator's response.

## CHAPTER V

## CONCLUSIONS

From observation of the strip chart recordings, attitude error increases and pilot control strategy changes markedly with increasing bending mode amplitude. The operator switches from a relay-like non-linear response to a combination of lower amplitude of pulsing and at times smooth tracking. Furthermore, significant bending mode excitation can develop at the lowest amplitude,  $1/3$  nom., under study.

The pilot describing functions show that as the bending mode amplitude increases, the pilot gain and phase lead compensation decrease. The decreased phase lead is best accounted for by greater subject dead-time delay.

The pilot attempts to track the oscillations that occur slightly below the bending mode natural frequency, however pilot response power decreases sharply at and above the natural frequency.

The RMS ratio of attitude error to disturbance signal substantiates quantitatively the increase of attitude error with respect to bending mode amplitude.

The subject performance is much poorer moving base than fixed base for all values of bending mode amplitude. The pilot exerts approximately the same control power in both cases. This results in a lower moving base gain.

Fixed base experiments including second order simulator dynamics and dead-zone plus the moving base display and control did not account for a major portion of the difference.

The best explanation seems to involve a combination of neglected simulator non-linearities, a poorly marked and less sensitive moving base display grid, and perhaps vestibular confusion and insensitivity to very small deflections.

The rate of increase of the attitude error with respect to bending mode amplitude was less rapid moving base compared to fixed base. The results were attributed to the simulator dead-zone and not to vestibular effects because the fixed base plus simulator dynamics results show a rate equal to that for moving base experiments.

For a given amplitude the bending mode with natural frequency of 5 rad/sec creates one-half the acceleration of the 7 rad/sec mode. Equal amplitudes for the two cause an approximately equal performance deterioration.

Possible spurious effects due to intersubject variance, subject knowledge of bending mode amplitude and order of occurrence, and fatigue were checked and not considered important.

For a given natural frequency and non-zero amplitude, the RMS ratios,  $\sqrt{e^2/d^2}$ , were typically 10% higher for the case of the low RMS disturbance signal compared with the

high RMS signal. The high RMS value was twice that of the low.

Highly simplified versions of two proposed vehicle augmentation and control stick filter schemes were studied experimentally. The results favor the one with stable missile rigid poles and single integration stick filter judged on the basis of attitude error performance. Both eliminated bending mode oscillations.

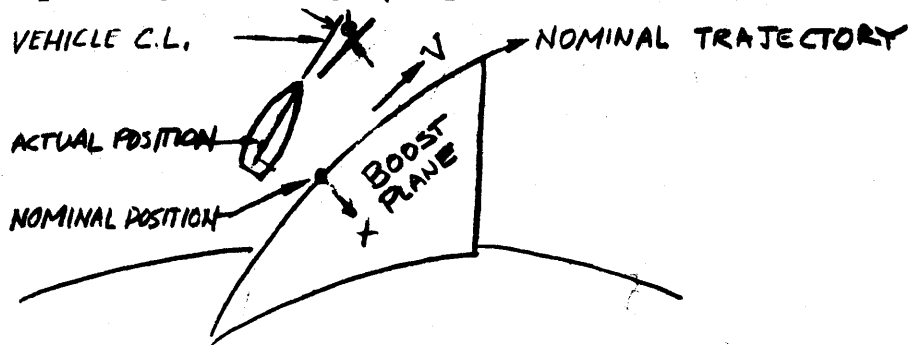
Because the single integration filtered out much more of the subjects response, the maximum available control power was arbitrarily increased by a factor of three. The attitude error difference may be due to this change.

A relatively low frequency first bending mode decreases pilot lead compensation and closed loop attitude performance in addition to creating structural problems. Significant effects develop at bending mode amplitudes equal to one-third that sensed at the Saturn V attitude station. Stick filters apparently solve the structural problem, but add phase lag in series with typically difficult dynamics. This requires effective stabilization of the vehicle dynamics to alleviate the pilot control problems in the presence of disturbance signals.

## APPENDIX A

## DERIVATION AND SIMPLIFICATION OF SIMULATION EQUATIONS

The equations of motion, parameters values, and following diagram are taken from Ref. 1. The equations of motion are linearized and valid for small perturbations about the booster's nominal trajectory. The equations are written with respect to a coordinate system moving at the booster velocity along the trajectory.



The rigid body equations are listed below:

$$\ddot{x} = -F_{\alpha} \alpha - F_{\phi} \phi_{rb} - F_{\beta} \beta \quad (\text{A } 1.0)$$

$$\dot{\phi}_{rb} = M_{\alpha} \alpha - M_{\beta} \beta \quad (\text{A } 2.0)$$

$$\alpha = \phi_{rb} + \frac{57.3}{V} \dot{x} \quad (\text{A } 3.0)$$

$$\ddot{\gamma}_{rb} = -F_{\alpha} \alpha - F_{\beta} \beta - \frac{1}{57.3} \ddot{\phi}_{rb} \quad (\text{A } 4.0)$$

Differentiating and rearranging equation (A 3.0) gives:

$$\ddot{x} = (\dot{\alpha} - \dot{\phi}_{rb}) \frac{V}{57.3} \quad (\text{A } 5.0)$$

After substitution into (A 1.0):

$$(\ddot{\alpha} - \dot{\phi}_{rb}) \frac{V}{57.3} = -F_{\alpha} \alpha - F_{\phi} \phi_{rb} - F_{\beta} \beta \quad (\text{A } 6.0)$$

Differentiating and rearranging equation (A 2.0):

$$\dot{\alpha} = \frac{1}{M_{\alpha}} (\ddot{\phi}_{rb} + M_{\beta} \dot{\beta}) \quad (\text{A } 7.0)$$

Substitution into (A 6.0) results in:

$$\frac{(\frac{1}{M_{\alpha}} \ddot{\phi}_{rb} + \frac{M_{\beta}}{M_{\alpha}} \dot{\beta} - \dot{\phi}_{rb}) \frac{V}{57.3}}{=} = -\frac{F_{\alpha}}{M_{\alpha}} (\ddot{\phi}_{rb} + M_{\beta} \dot{\beta}) - F_{\phi} \phi_{rb} - F_{\beta} \beta \quad (\text{A } 8.0)$$

Rearranging (A 8.0):

$$\frac{\frac{V}{57.3 M_{\alpha}} \ddot{\phi}_{rb} + \frac{F_{\alpha}}{M_{\alpha}} \ddot{\phi}_{rb} - \frac{V}{57.3} \dot{\phi}_{rb} + F_{\phi} \phi_{rb}}{=} = -\frac{M_{\beta}}{M_{\alpha}} \frac{V}{57.3} \dot{\beta} - F_{\beta} \beta - F_{\alpha} \frac{M_{\beta}}{M_{\alpha}} \beta \quad (\text{A } 9.0)$$

Using Laplace operator notation:

$$\frac{\phi_{rb}}{\beta} = \frac{(\frac{M_{\beta}}{M_{\alpha}} \frac{V}{57.3} p + F_{\beta} + F_{\alpha} \frac{M_{\beta}}{M_{\alpha}})}{(\frac{V}{57.3 M_{\alpha}} p^3 + \frac{F_{\alpha}}{M_{\alpha}} p^2 - \frac{V}{57.3} p + F_{\phi})} \quad (\text{A } 10.0)$$

$$= -M_{\beta} \frac{(p + \frac{M_{\alpha}}{M_{\beta}} \frac{F_{\beta}}{V} 57.3 + F_{\alpha} \frac{57.3}{V})}{(p^3 + \frac{57.3}{V} F_{\alpha} p^2 - M_{\alpha} p + \frac{57.3 M_{\alpha}}{V} F_{\phi})} \quad (\text{A } 10.1)$$

At maximum dynamic pressure the parameters have the following values:

$$\begin{array}{ll} M_{\alpha} = .141/\text{sec}^2 & F_{\phi} = .36 \text{ meters}/\text{sec}^2/\text{deg} \\ M_{\beta} = 1.15/\text{sec} & F_{\alpha} = .13 \text{ meters}/\text{sec}^2/\text{deg} \\ V = 486 \text{ m}/\text{sec} & F_{\beta} = .30 \text{ meters}/\text{sec}^2/\text{deg} \end{array}$$

After substitution of these values (A 10.1) becomes:

$$\frac{\phi_{rb}}{\beta} = - 1.15 \frac{(p + .02)}{(p^3 + .0153p^2 - .14p + .0060)} \quad (\text{A } 10.2)$$

$$= - 1.15 \frac{(p + .02)}{(p - .34)(p + .40)(p - .04)} \quad (\text{A } 10.3)$$

Considering only  $\frac{(p + .02)}{(p - .04)}$  for  $p = j\omega > .4 \text{ rad}/\text{sec}$ :

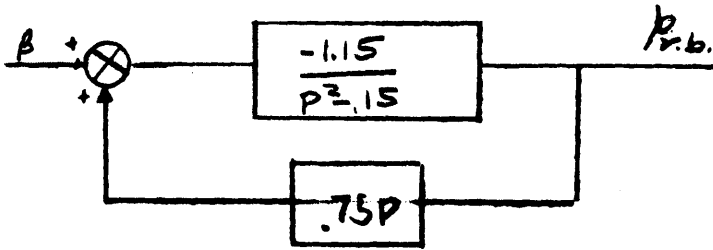
$$\left| \frac{p + .02}{p - .04} \right| \approx 1 \text{ and } \angle(p + .02) - \angle(p - .04) \approx 0^\circ$$

For simulation purposes (A 10.3) was simplified accordingly:

$$\frac{\phi_{rb}}{\beta} \approx - \frac{1.15}{(p - .34)(p + .40)} \quad (\text{A } 11.0)$$

$$\approx - \frac{1.15}{p^2 - .15} \quad (\text{A } 11.1)$$

If rate compensation is added, the feedback polarity must be as shown to decrease the instability:



Then:

$$\phi_{rb} = -\frac{1.15}{p^2 - .15} \beta - \frac{.75p(1.15)}{p^2 - .15} \phi_{rb} \quad (\text{A } 12.0)$$

After rearrangement:

$$\phi_{rb} (p^2 + .86p - .15) = -1.15\beta \quad (\text{A } 13.0)$$

$$\frac{\phi_{rb}}{\beta} = -\frac{1.15}{(p^2 + .86p - .15)} \quad (\text{A } 14.0)$$

$$= -\frac{1.15}{(p + 1.00)(p - .15)} \quad (\text{A } 14.1)$$

The following equations describe the flexible body mode:

$$\ddot{\eta} + 2\xi\omega_{nbd}\dot{\eta} + \omega_{nbd}^2\eta = K_{11}\beta + K_{21}\beta \quad (\text{A } 15.0)$$

$$\phi_{bd} = K_{31}\eta \quad (\text{A } 16.0)$$

Combining and rearranging:

$$\frac{\phi_{bd}}{\beta} = \frac{K_{31}K_{21}(p^2 + \frac{K_{11}}{K_{21}})}{(p^2 + 2\xi\omega_{nbd}p + \omega_{nbd}^2)} \quad (\text{A } 17.0)$$

The values for these parameters at maximum dynamic pressure are:

$$\begin{aligned} K_{11} &= .46/\text{deg-sec} & \xi &= .005 \\ K_{21} &= .00077/\text{deg} & \omega_{\text{nb}} &= 7.33 \text{ rad/sec} \\ K_{31} &= 8.6 \text{ deg} \end{aligned}$$

After substitution:

$$\frac{\phi_{\text{bd}}}{\beta} = \frac{.0066(p^2 + (24.4)^2)}{(p^2 + .01(7.33)p + (7.33)^2)} = \frac{K(p^2 + \omega_z^2)}{(p^2 + .01\omega_p p + \omega_p^2)} \quad (\text{A } 18.0)$$

For convenience,  $\omega_z$  was made equal to  $3\omega_p$  for all values of  $\omega_p$  under study.

The total attitude error,  $\phi_{\text{total}}$ , equals the sum of the rigid body and flexible body contributions, therefore:

$$\frac{\phi_{\text{tot}}}{\beta} = \frac{-1.15}{(p+1.00)(p-.15)} + \frac{K(p^2 + (3\omega_{\text{nb}})^2)}{(p^2 + .01\omega_{\text{nb}}p + \omega_{\text{nb}}^2)} \quad (\text{A } 19.0)$$

$$= \frac{-1.15(p^2 + .01\omega_{\text{nb}}p + \omega_{\text{nb}}^2) + K(p^2 + (3\omega_{\text{nb}})^2)(p+1.00)(p-.15)}{(p+1.00)(p-.15)(p^2 + .01\omega_{\text{nb}}p + \omega_{\text{nb}}^2)} \quad (\text{A } 20.0)$$

The root locus technique was used to factor the numerator. A separate root locus plot appears for both bending mode frequencies, (see Fig. A1 and A2). The numerator must be written in the following form to apply the technique:

$$1 - \frac{1.15(p^2 + .01\omega_{\text{nb}}p + \omega_{\text{nb}}^2)}{K(p^2 + (3\omega_{\text{nb}})^2)(p - .15)(p + 1.00)} = 0 \quad (\text{A } 21.0)$$

From inspection, the  $0^\circ$  criterion must be used, and the root locus gain equals  $1.15/K$ .

Roots have been located for the appropriate values of  $K$  on the two plots. The results are listed in Chapter II in transfer function form. The root locus gains corresponding to bending amplitudes are listed below:

K	K Root Locus
.0022	522.7
.0066 (nom.)	174.2
.0132	87.1
.0264	43.6

The root locus gain is related to the spirule reading accordingly:

$$K_{r1} = (\text{Spirule reading}) S^{p-q} \frac{|q_1 q_2|}{|p_1 p_2 p_3 p_4|} \quad (\text{A } 22.0)$$

where  $S$  is scale factor equal to the number of radians/sec represented by 5" on the plot and  $p_i$  and  $q_i$  are the locations of the poles and zeroes.

$$\text{For } \omega_n = 5, \frac{|q_1 q_2|}{|p_1 p_2 p_3 p_4|} \approx \frac{|(5_j)(-5_j)|}{|(-.15)(1.00)(15_j)(-15_j)|} = \frac{25}{33.75} = .74$$

$$\omega_n = 7, \frac{|q_1 q_2|}{|p_1 p_2 p_3 p_4|} = \frac{|(7_j)(-7_j)|}{|(-.15)(1.00)(21_j)(-21_j)|} = \frac{49}{66.15} = .74$$

In this case  $S = 20$ , so the spirule readings and the bending mode amplitudes have the following relationship:

$$(\text{spirule reading}) = \frac{|p_1 p_2 p_3 p_4|}{|q_1 q_2|} \frac{1}{S^{p-q}} \frac{1.15}{K} \quad (\text{A } 23.0)$$

Finally:

K	Spirule Reading
.0022	1.77
.0066	.59
.0132	.29
.0264	.15

Jex and Teper augment the dynamics of the Saturn V by feeding back both attitude rate and position. The sum of the control stick filter output and the feedback signal passes through two first order lags with break frequencies at 5 rad/sec. This filtered signal provides the command to the engine gimbal. The complicated closed loop transfer function including two bending modes as taken from Ref. 2 appears below:

$$\frac{\phi_{\text{attitude gyro}}}{\beta_{\text{stick filter}}} = \frac{4,900(s+.019)(s+4.5)(s-4.6) \binom{0.0050}{12} \binom{0.00066}{21}}{(s+0.035)(s+.62)(s+6)(s+30) \binom{0.56}{2} \binom{0.038}{7.2} \binom{0.018}{12} \binom{0.30}{30}} \quad (\text{A } 24.0)$$

where  $\binom{0.30}{30}$  denotes  $(p^2 + 2(.30)p + 30^2)$

The dominant rigid body modes are now stable and have a natural frequency of 2 rad/sec and a damping ratio,  $\xi = .56$ .

In order to reduce the complexity of this set of dynamics to a level equal to the previous work, the two dominant rigid body poles were placed in parallel with the simulated first bending mode.

The extreme simplification not only reduces the complexity, but also, the difficulty of the dynamics proposed by Teper and Jex.

However, in spite of this fact, a first approximation to a realizable set of stabilized Saturn V rigid body dynamics has been selected.

The new set of missile dynamics has the following form:

$$\frac{\phi_{\text{tot}}}{\beta} = \frac{4k}{p^2 + 2(.56)2p + 2^2} + \frac{.0066 (p^2 + 21^2)}{(p^2 + 2(.005)7p + 7^2)} \quad (\text{A } 25.0)$$

The natural frequency of the bending mode was placed at 7 rad/sec and  $K = .0066 = \text{nom.}$  to correspond closely with the Saturn V design conditions. The value of the remaining parameter,  $k$ , was selected after initial experiments with this system. The basis for the choice is discussed in Chapter IV. With the selected value of  $k = .85$ , equation (A 25.0) becomes:

$$\frac{\phi_{\text{tot}}}{\beta} = \frac{3.4(p^2 + (.01)7p + 7^2) + .0066(p^2 + 21^2)(p^2 + 2(.56)2p + 2^2)}{(p^2 + 2(.56)2p + 2^2)(p^2 + (.01)7p + 7^2)} \quad (\text{A } 26.0)$$

After placing the numerator in a form suitable for solution by the root locus technique:

$$1 - \frac{3.4}{.0066} \cdot \frac{(p^2 + (.01)7 p + 7^2)}{(p^2 + 21^2)(p^2 + 2(.56)2 p + 2^2)} = 0 \quad (\text{A } 27.0)$$

After solution of the root locus:

$$\frac{\phi_{\text{tot}}}{\beta} \approx \frac{.0066(p-11)(p+15.5)(p^2+(10.5)^2)}{(p^2+2(.56)2p+2^2)(p^2+.01(7)p+7^2)} \quad (\text{A } 28.0)$$

## APPENDIX B

## PILOT DESCRIBING FUNCTION MEASUREMENT TECHNIQUE

The pilot describing functions were computed by the following equation:<sup>5</sup>

$$Y_p(s) = \frac{\Phi_{13}(\omega)}{\Phi_{12}(\omega)} \quad (\text{B1.0})$$

where:

$\Phi_{13}(\omega)$  = cross power spectral density of the input disturbance signal and the operator's response.

$\Phi_{12}(\omega)$  = cross power spectral density of the input disturbance signal and the displayed error.

The operator's response contains a part correlated with the input disturbance signal and an uncorrelated remnant. The degree of correlation determines how well a describing function accounts for his behavior.

This correlation is measured by the following ratio:

$$\rho^2 = \frac{|\Phi_{13}(\omega)|^2}{\Phi_{11}(\omega) \Phi_{33}(\omega)} \quad (\text{B2.0})$$

where:

$\phi_{11}(\omega)$  = input disturbance signal power spectral density

$\phi_{33}(\omega)$  = operator's response power spectral density.

If  $\rho^2$  is near unity the describing function is a close approximation to the operator's behavior.

A program, written by the staff of Health Sciences Computing Facility, UCLA, and made available to the Man-Vehicle Control Laboratory by Ames Research Center, NASA, was used to compute the necessary power spectrums. The program was modified in the Man-Vehicle Control Laboratory to compute the describing function by (B1.0).<sup>6</sup>

This method computes the power spectral estimates of an analog signal T seconds long by sampling every  $\Delta T$  seconds.

A total of  $M = T/\Delta T$  points are available for computation. The correlation function  $\phi(\tau)$  of the sampled signal is computed for m lags of  $\Delta T$ .

Under these conditions:

1. The sampled data will have no spectral power above a frequency  $\omega_{\text{high}}$  where:

$$\omega_{\text{high}} = \frac{\pi}{\Delta T} \quad (\text{B3.0})$$

2. The spectral density will be computed at m equally spaced frequencies between 0 and  $\omega_{\text{high}}$ . Hence the frequency resolution will be:

$$\Delta\omega = \frac{\pi}{m \Delta T}$$

3. The probable error of the computed spectral error will be:

$$\epsilon = \sqrt{\frac{m}{M}}$$

If N independent spectral densities are averaged, the probable error is reduced to:

$$\epsilon = \sqrt{\frac{m}{NM}}$$

For this work the following values were chosen:

$$T = 70 \text{ sec}$$

$$\Delta T = 0.1 \text{ sec}$$

$$M = 700$$

$$N = \text{typically } 5$$

For these values:

$$\omega_{\text{high}} = 5 \text{ cps}$$

$$\Delta\omega \approx .07 \text{ cps}$$

$$M = 700 \text{ points}$$

$$\epsilon = \sqrt{\frac{70}{5(700)}} \approx .14$$

## BIBLIOGRAPHY

1. Hardy, G. H., West, J. V., and Gunderson, R. W., "Evaluation of Pilot's Ability to Stabilize a Flexible Launch Vehicle During First-Stage Boost," NASA TN D-2807, May 1965.
2. Jex, H. R. and Teper, G. L., Personal communication with author..
3. Lukens, D. R., Schmitt, A. F., and Broucek, G. T., "Approximate Transfer Functions for Flexible-Booster-and-Autopilot Analysis," WADC TR-61-93, April 1961.
4. McNemar, Q., Psychological Statistics, John Wiley and Sons, Inc., 1962.
5. McRuer, D. T. and Krendel, E. S., "Dynamic Response of Human Operators," WADC TR56-524, August 1957.
6. Meiry, J. L., "The Vestibular System and Human Dynamic Space Orientation," Doctoral Thesis, Man-Vehicle Control Laboratory, Massachusetts Institute of Technology, June 1965.
7. Teper, G. L., and Jex, H. R., "Synthesis of Manned Booster Control Systems Using Mathematical Pilot Models," Sixth Annual Symposium of the Professional Group on Human Factors in Electronics, IEEE, May 1965.

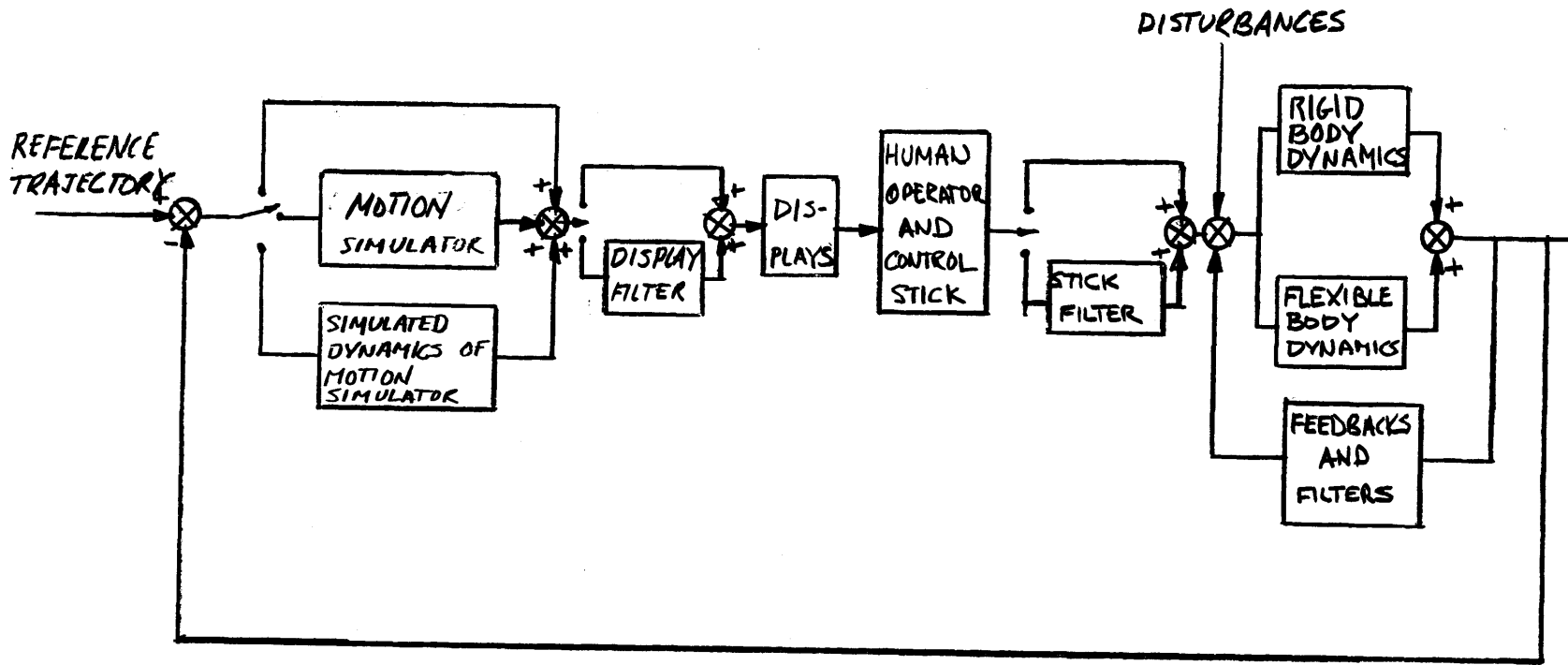


FIG. 1 GENERAL BLOCK DIAGRAM FOR MAN-BOOSTER CONTROL PROBLEM

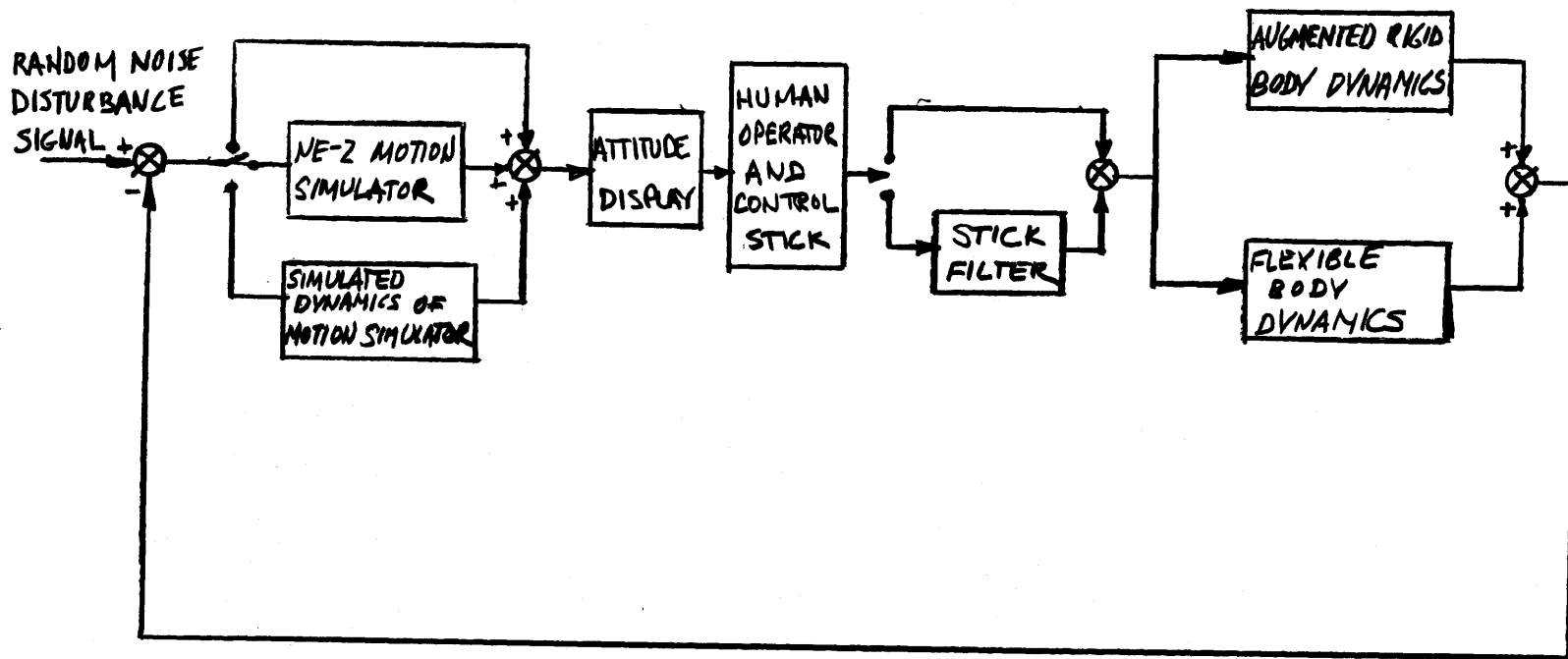
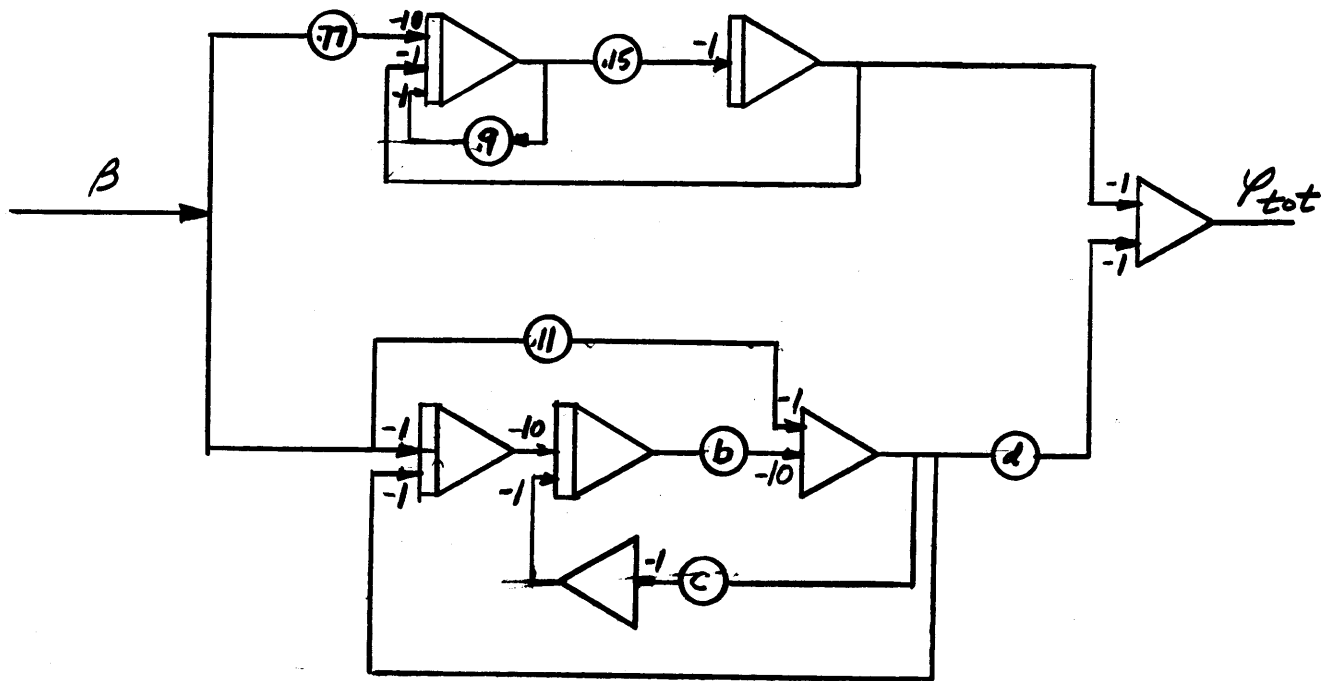
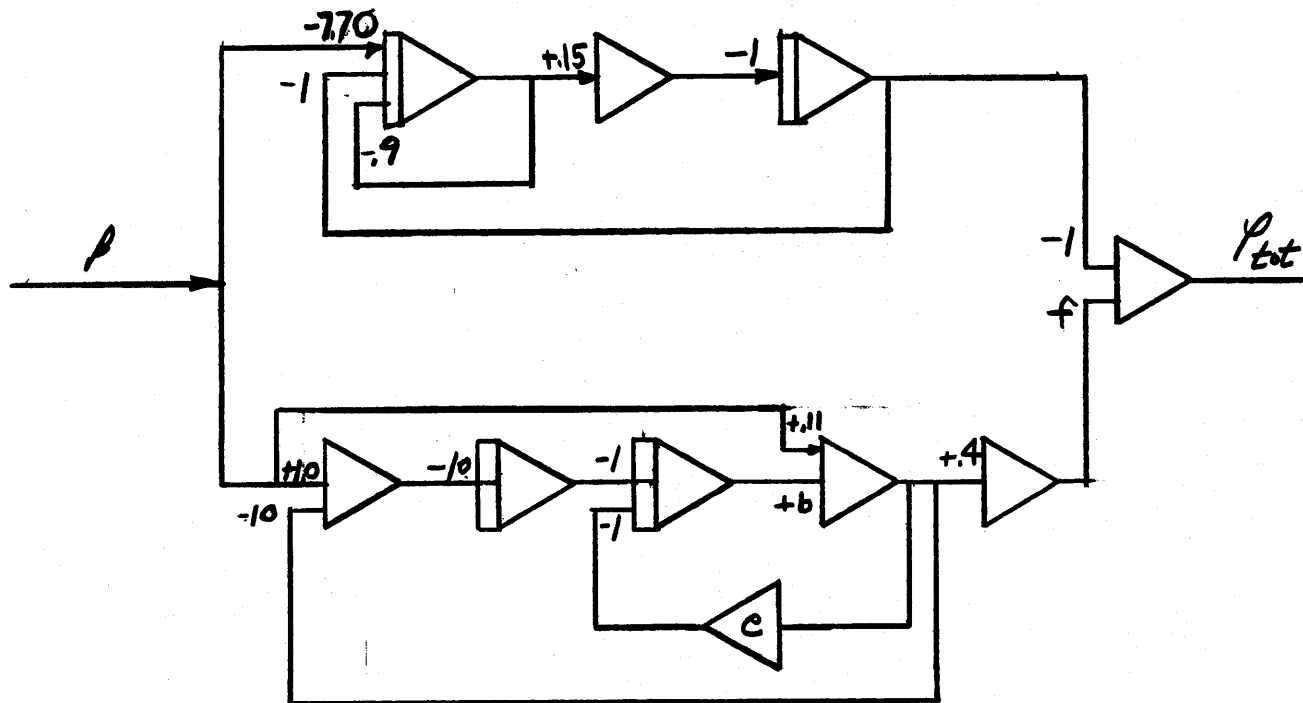


FIG. 2. BLOCK DIAGRAM FOR THE MAN-BOOSTER CONTROL PROBLEM AS STUDIED IN THIS INVESTIGATION



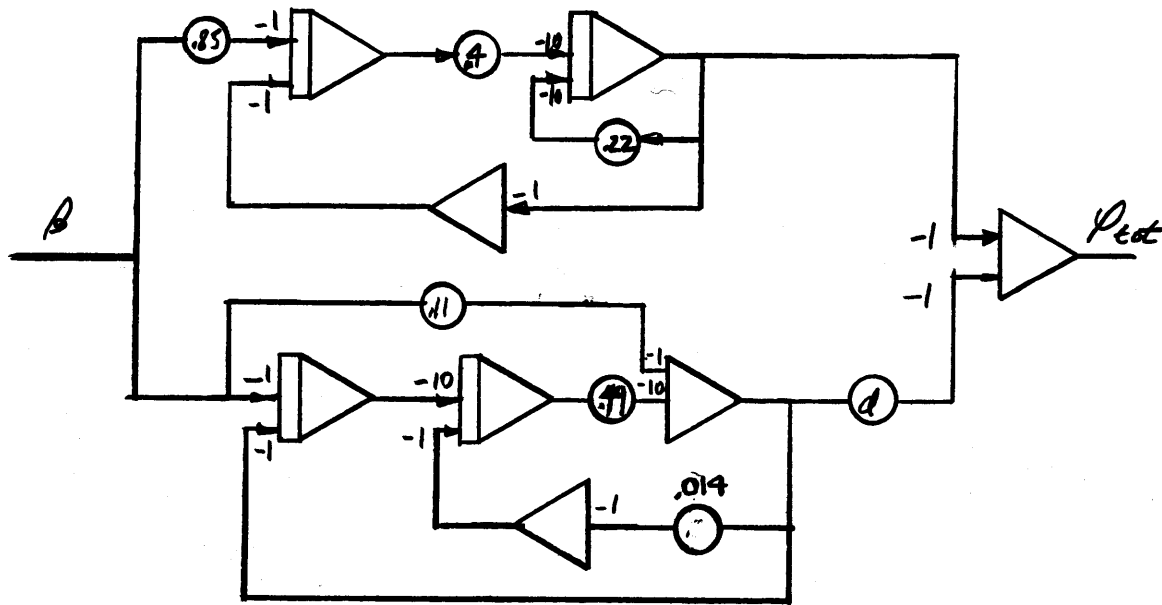
$$\frac{Y_{tot}}{B} = \frac{-1.15}{p^2 + .86p - .15} + \frac{.11d [p^2 + \frac{100b}{.11}]}{[p^2 + 10cbp + 100b]}$$

FIG. 3 ANALOG COMPUTER PATCHING PROGRAM FOR FIXED BASE EXPERIMENTS



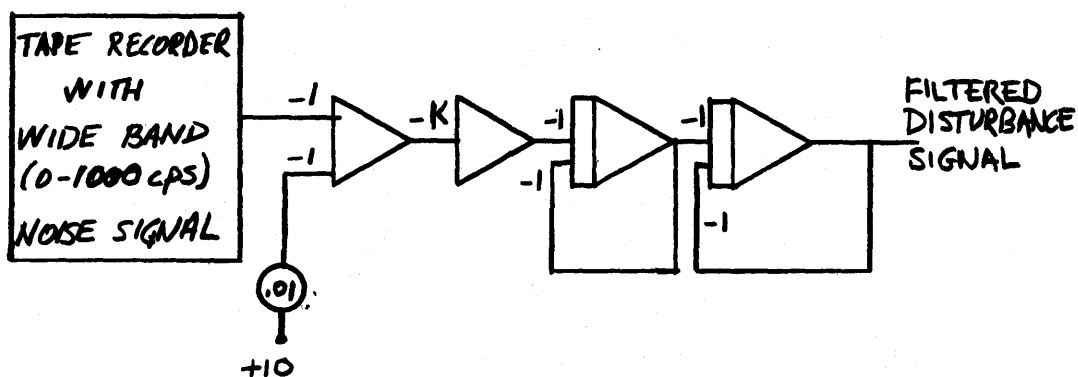
$$\frac{p_{tot}}{p} = \frac{-1.15}{[p^2 + 1.86p - 15]} + \frac{.11(4)[p^2 + \frac{100b}{.11}]}{[p^2 + cbp + 100b]}$$

FIG. 4 ANALOG COMPUTER PATCHING PROGRAM FOR MOVING BASE EXPERIMENTS



$$\frac{y_{out}}{B} = \frac{-0.85(4)}{(p^2 + 2(54)2p + 2^2)} + \frac{.0066(p^2 + 21^2)}{(p^2 + 2(005)7p + 7^2)}$$

FIG. 5 ANALOG COMPUTER PATCHING PROGRAM FOR A MODIFIED VERSION OF THE AUGMENTED DYNAMICS OF TEPER & JEX



$K=7.2$  ; FIXED BASE, HIGH RMS DISTURBANCE (1 VOLT =  $1^\circ$ )

$=3.6$  ; FIXED BASE, LOW RMS DISTURBANCE

$=2A$  ; MOVING BASE (1 VOLT  $\approx 3^\circ$ )

FIG 6 ANALOG COMPUTER PATCHING PROGRAM USED TO SHAPE THE SPECTRUM OF THE DISTURBANCE SIGNAL

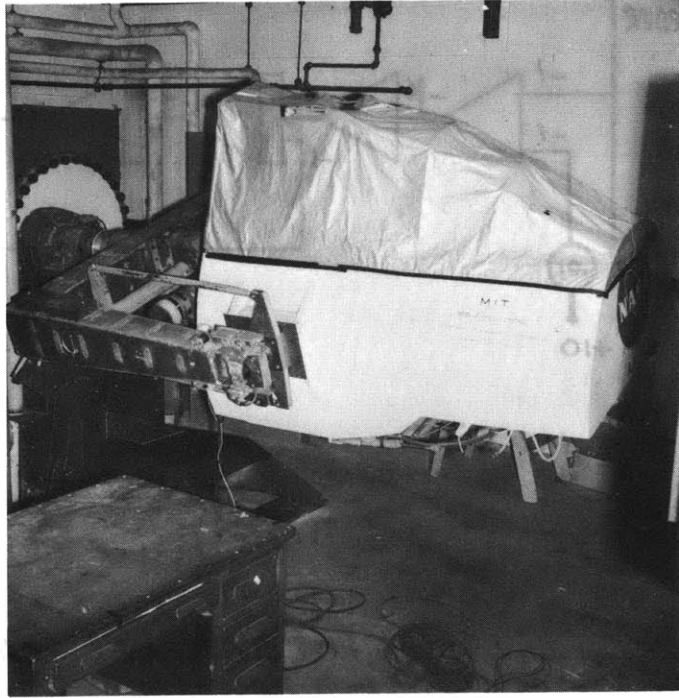


FIG. 7.- NE-2 MOTION SIMULATOR

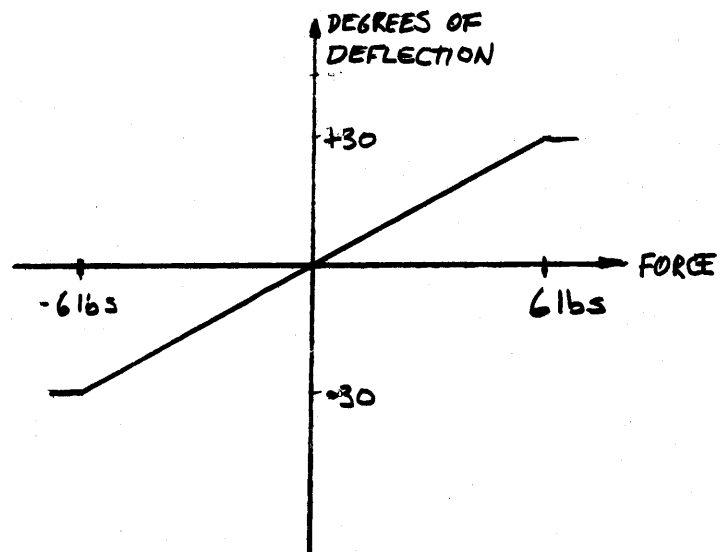


FIG. 8a FIXED BASE CONTROL STICK CHARACTERISTICS

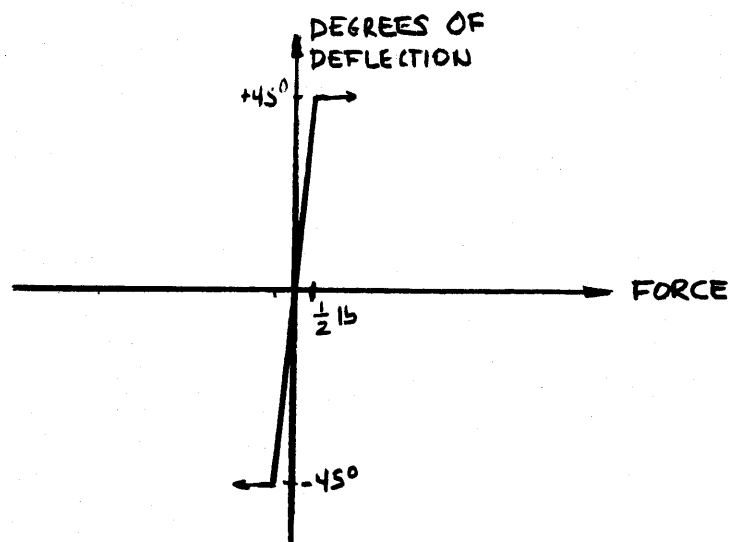


FIG. 8b MOVING BASE CONTROL STICK CHARACTERISTICS

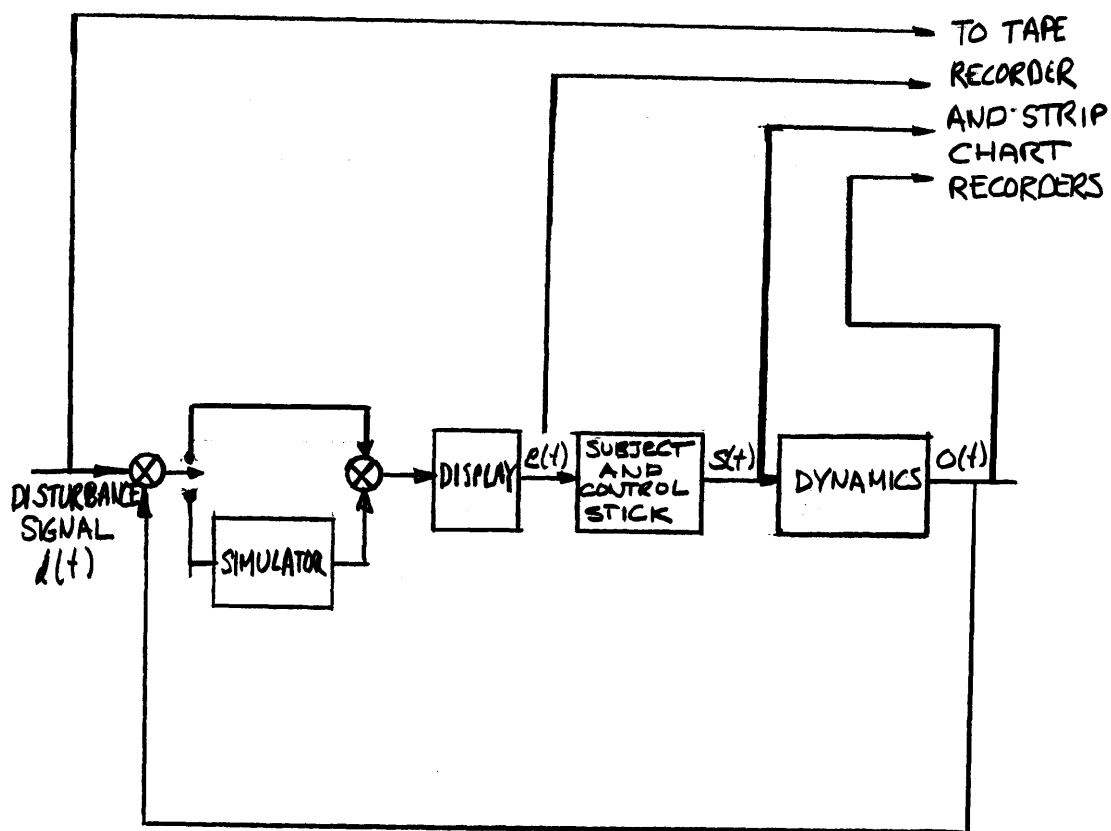


FIG 9 - BLOCK DIAGRAM SHOWING CONTROL SYSTEM SIGNALS RECORDED ON STRIP CHART AND TAPE RECORDERS



FIG. 10.- SUBJECT POSITION AND EQUIPMENT LOCATION FOR  
FIXED BASE EXPERIMENTS

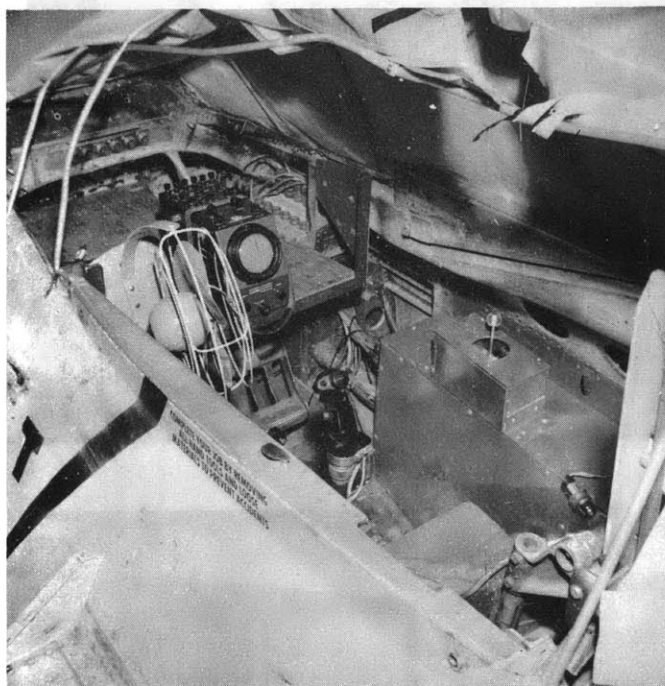


FIG. 11.- SUBJECT POSITION, CONTROL STICK AND DISPLAY LOCATION FOR MOVING BASE EXPERIMENTS

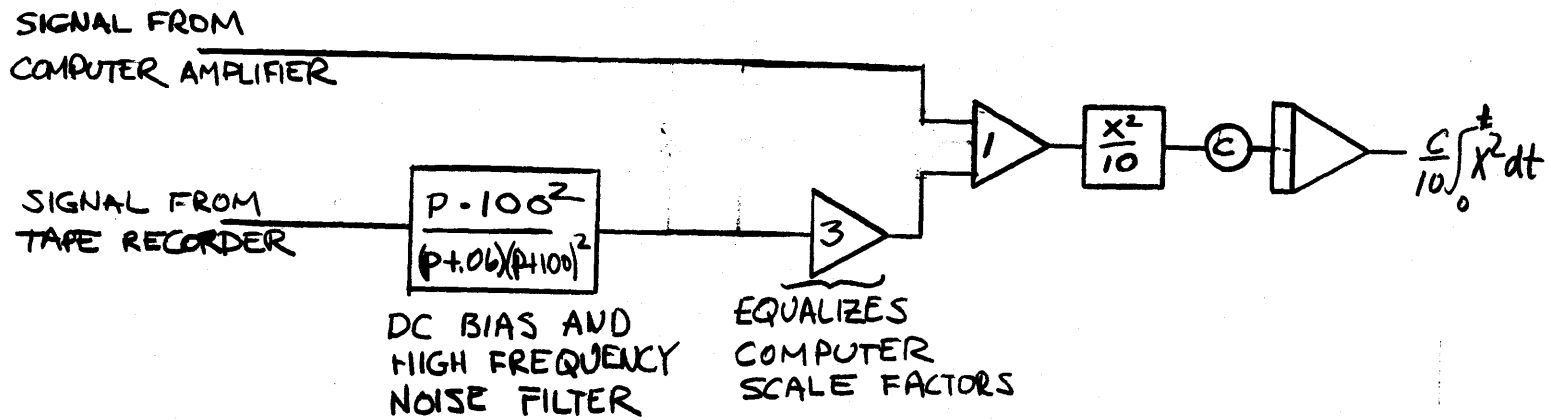
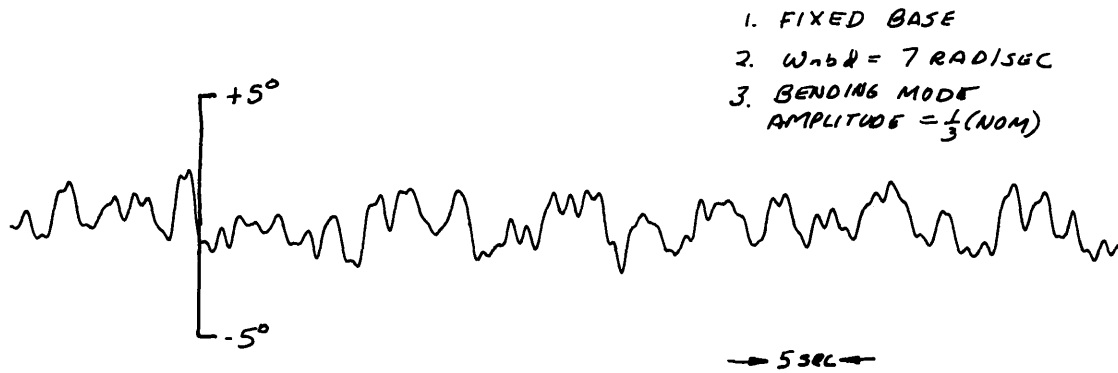
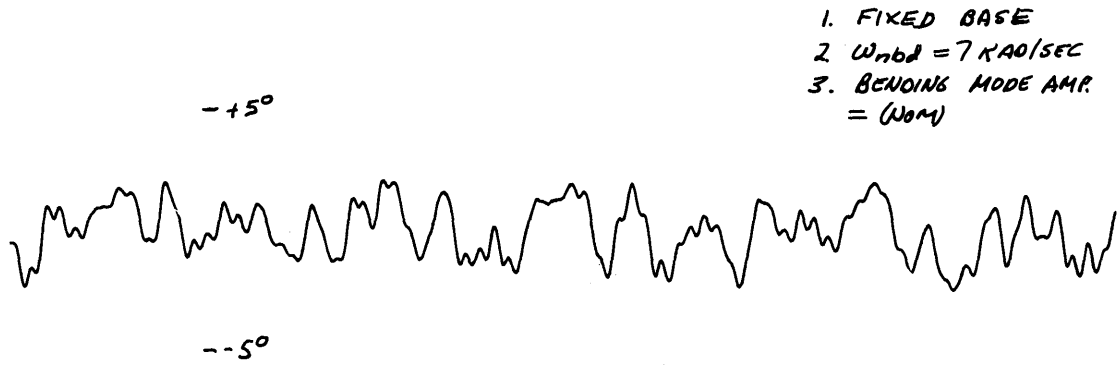


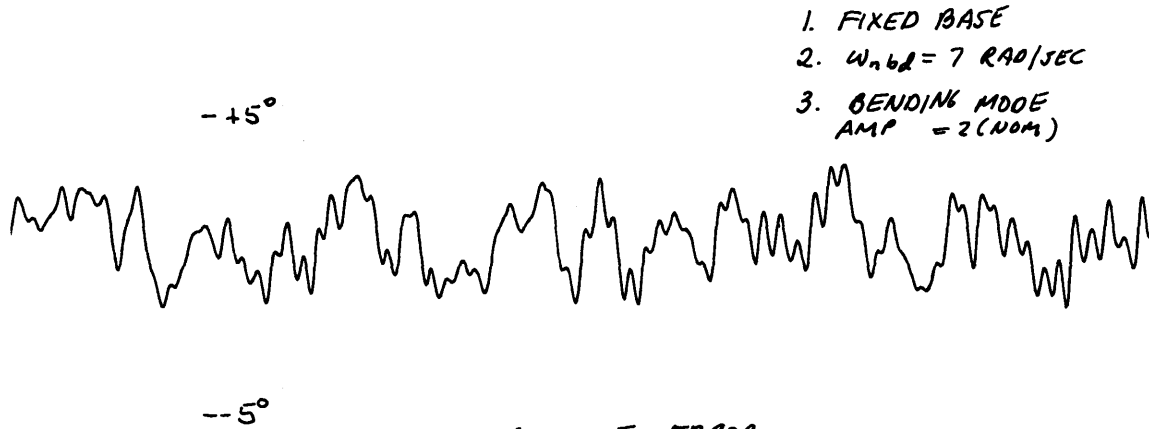
FIG. 12- ANALOG PATCHING PROGRAM FOR INTEGRAL SQUARE ERROR CALCULATIONS



ATTITUDE ERROR



ATTITUDE ERROR



ATTITUDE ERROR

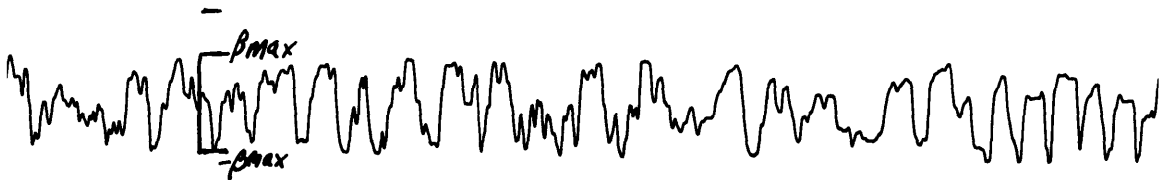
FIG. 13.- STRIP CHART RECORDINGS OF ATTITUDE ERROR

1. FIXED BASE
2.  $\omega_{bd} = 7 \text{ RAD/SEC}$
3. BENDING MODE  
AMP =  $\frac{1}{3} \text{ NOM}$



CONTROL STICK RESPONSE

1. FIXED BASE
2.  $\omega_{bd} = 7 \text{ RAD/SEC}$
3. BENDING MODE  
AMP =  $2(\text{NOM})$



CONTROL STICK RESPONSE

1. FIXED BASE
2.  $\omega_{bd} = 7 \text{ RAD/SEC}$
3. BENDING MODE  
AMP =  $2(\text{NOM})$



CONTROL STICK RESPONSE

FIG. 14.- STRIP CHART RECORDINGS OF PILOT RESPONSE



TABLE 2

EXPERIMENTAL CONDITIONS: FIXED BASE,  $\omega_{hd} = 7 \text{ RAD/SEC}$

PILOT DESCRIBING FUNCTION DATA

AMPLITUDE RATIO

PHASE ANGLE (LEAD +)

BENDING MODE AMPLITUDE	FREQ. $\omega$ RADIANS No OF TRACKING RUNS AVERAGED	AMPLITUDE RATIO									PHASE ANGLE (LEAD +)							
		.45	.90	1.34	1.80	2.24	2.70	3.14	3.58		.45	.90	1.34	1.80	2.24	2.70	3.14	3.58
0	5	2.14	2.62	3.58	4.15	4.58	4.65	4.77	5.39		10	18	26	23	23	22	17	15
$\frac{1}{3}$ NOM	5	1.78	2.08	2.88	3.34	3.78	4.01	5.27	4.25		11	22	27	24	21	17	15	7
NOM	6	1.35	1.53	2.02	2.42	2.76	2.90	2.90	3.10		15	20	24	19	17	13	6	0
2 NOM	5	1.00	1.10	1.51	1.76	1.87	2.03	2.30	2.34		17	21	20	15	12	5	2	-10
		CORRELATION COEFFICIENT																
0	5	.71	.70	.77	.82	.83	.73	.61	.42									
$\frac{1}{3}$ NOM	5	.72	.72	.82	.84	.85	.82	.72	.52									
NOM	6	.71	.72	.80	.82	.81	.70	.56	.39									
2 NOM	5	.72	.75	.75	.83	.78	.73	.70	.40									

TABLE 3

EXPERIMENTAL CONDITIONS: MOVING BASE,  $\omega_{nbd} = 7$  RAD/SEC

PILOT DESCRIBING FUNCTION DATA

AMPLITUDE RATIO

PHASE ANGLE (LEAD +)

BENDING MODE AMPLITUDE	FREQ. IN RADIANS NO OF TRACKING RONS WERES	AMPLITUDE RATIO								PHASE ANGLE (LEAD +)							
		.45	.90	1.35	1.80	2.24	2.70	3.14	3.58	.45	.90	1.34	1.80	2.24	2.70	3.14	3.58
0	4	.82	.86	1.02	1.18	1.52	1.66	1.86	2.01	11	20	20	17	8	2	-10	-6
.55 NOM	5	.78	.83	.96	1.11	1.44	1.51	1.56	1.58	21	25	26	24	8	5	-6	-8
1.25 NOM	5	.65	.73	.81	.93	1.27	1.45	1.41	1.44	7	19	21	19	-6	-6	-13	-12
2.50 NOM	5	.59	.62	.72	.86	1.05	1.23	1.27	1.25	10	15	15	12	-4	-12	-30	-18
		CORRELATION COEFFICIENTS															
0	4	.37	.78	.81	.64	.50	.49	.42	.35								
.55 NOM	5	.37	.79	.79	.45	.41	.45	.43	.36								
1.25 NOM	5	.48	.80	.83	.57	.37	.41	.27	.29								
2.50 NOM	5	.32	.72	.74	.54	.30	.35	.18	.12								

TABLE 4

EXPERIMENTAL CONDITIONS: MOVING BASE,  $\omega_{cmd} = 5 \text{ RAD/SEC}$

PILOT DESCRIBING FUNCTION DATA

AMPLITUDE RATIO

PHASE ANGLE (LEAD)

BENDING MODE AMPLITUDE	FREQ. IN RAD/SEC NO OF TRACKING RUNS AVERAGED	AMPLITUDE RATIO								PHASE ANGLE (LEAD)							
		.45	.90	1.35	1.80	2.24	2.70	3.14	3.58	.45	.90	1.35	1.80	2.24	2.70	3.14	3.58
0	3	.99	1.14	1.38	1.63	1.86	2.08	2.26	2.27	12	32	34	32	26	19	16	-4
1.25 NOM	5	.88	.86	1.04	1.18	1.34	1.61	2.00	2.13	37	32	31	29	27	18	14	9
2.5 NOM	5	.64	.67	.82	.87	1.03	1.27	1.34	1.29	27	27	30	27	18	10	10	7
3.2 NOM	5	.63	.65	.74	.84	.97	1.03	1.27	1.28	5	18	20	18	11	5	-8	9
3.8 NOM	4	.54	.64	.71	.84	.93	1.06	1.12	1.18	13	20	25	26	16	9	-2	5
		CORRELATION COEFFICIENT															
0	3	.41	.74	.84	.72	.46	.38	.42	.42								
1.25 NOM	5	.29	.68	.77	.67	.51	.49	.32	.25								
2.5 NOM	5	.32	.70	.73	.56	.35	.35	.34	.21								
3.2 NOM	5	.42	.72	.81	.71	.48	.26	.25	.25								
3.8 NOM	4	.32	.71	.80	.60	.24	.22	.08	-								

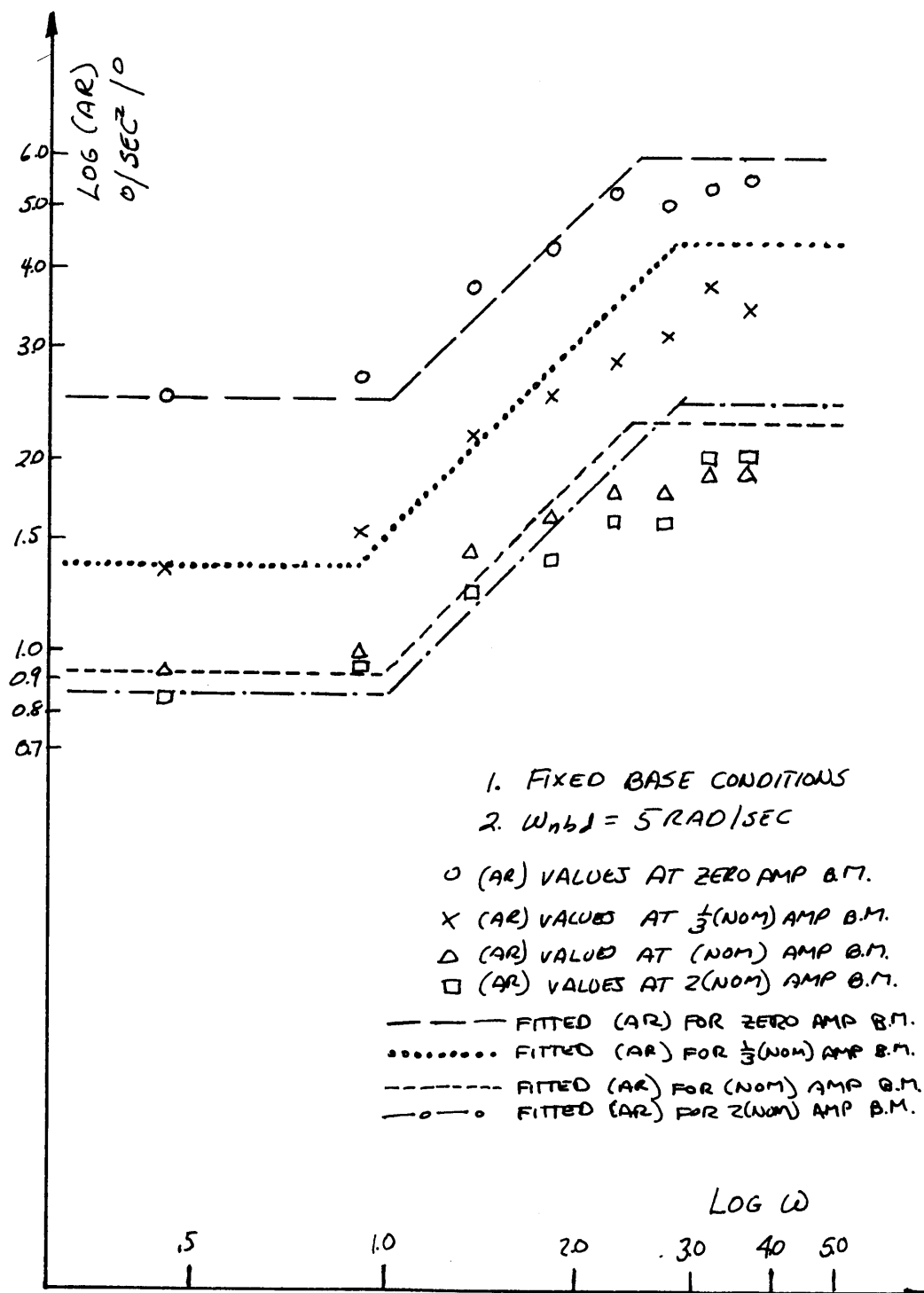


FIG. 15 — PLOT OF AMPLITUDE RATIO DATA FROM TABLE 1  
FOR SUBJECT DESCRIBING FUNCTION

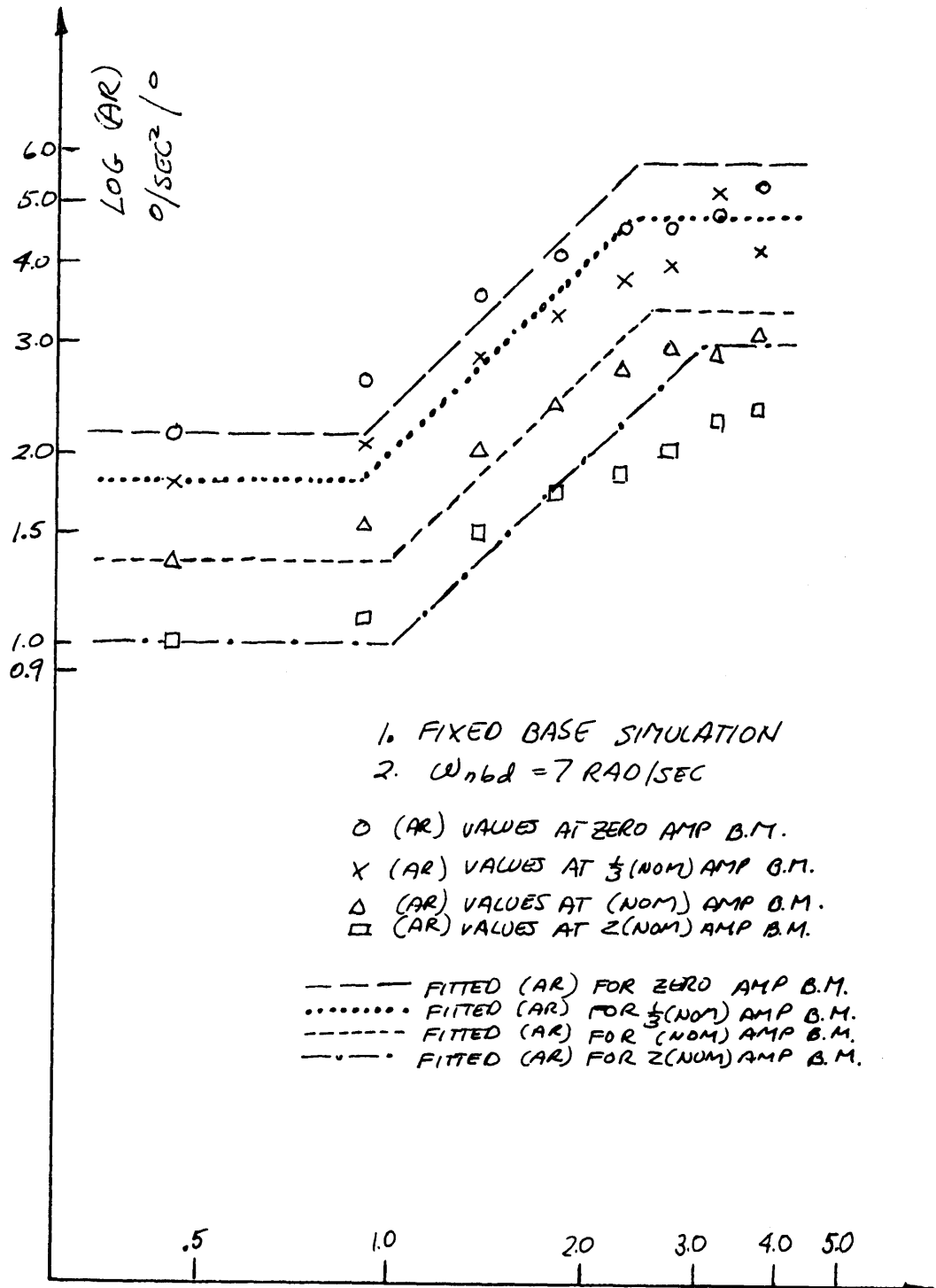


FIG. 16 - PLOT OF AMPLITUDE RATIO DATA FROM TABLE 2  
 FOR SUBJECT DESCRIBING FUNCTION

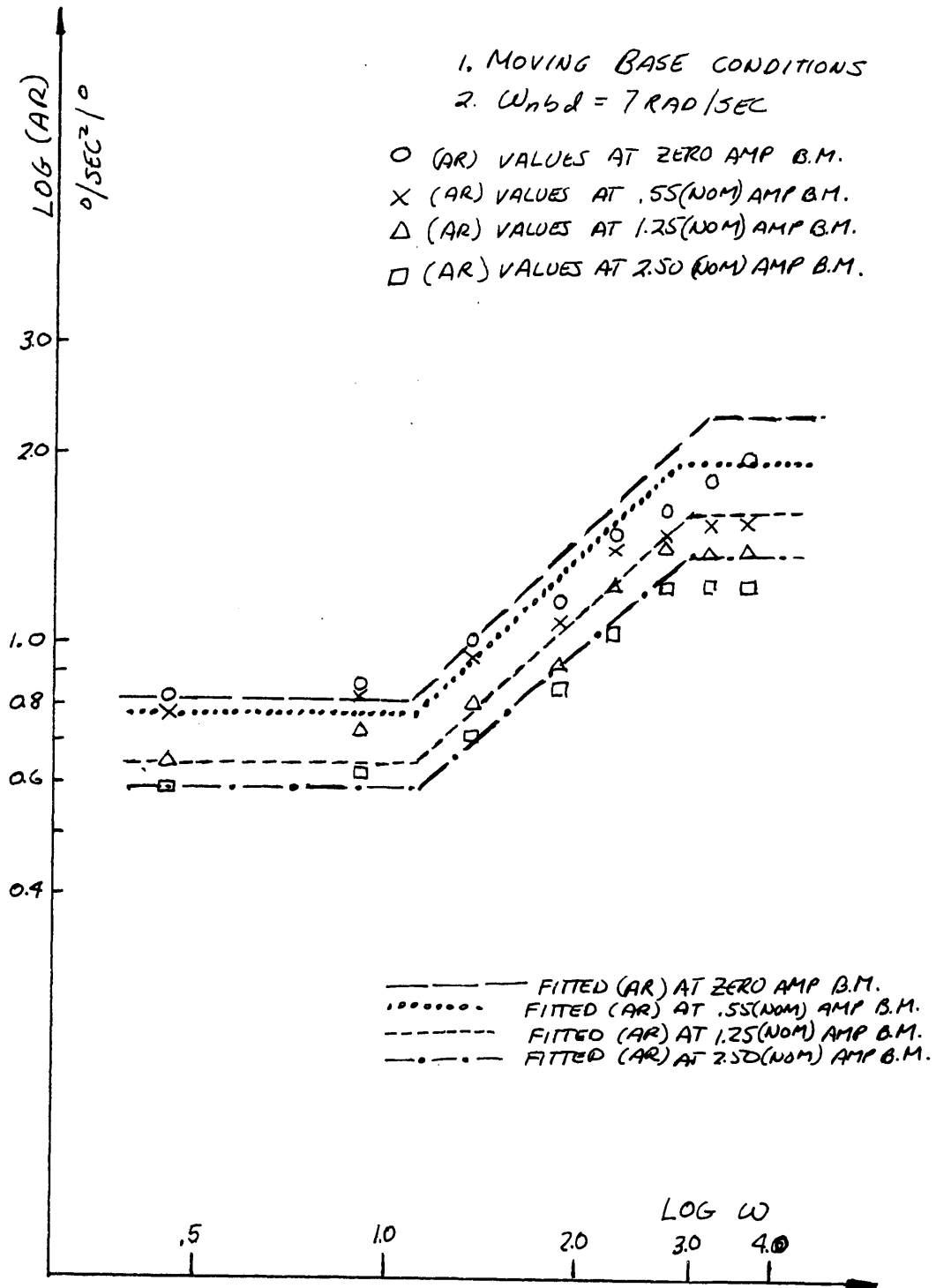


FIG. 17- PLOT OF AMPLITUDE RATIO DATA FROM TABLE 3  
FOR SUBJECT DESCRIBING FUNCTION

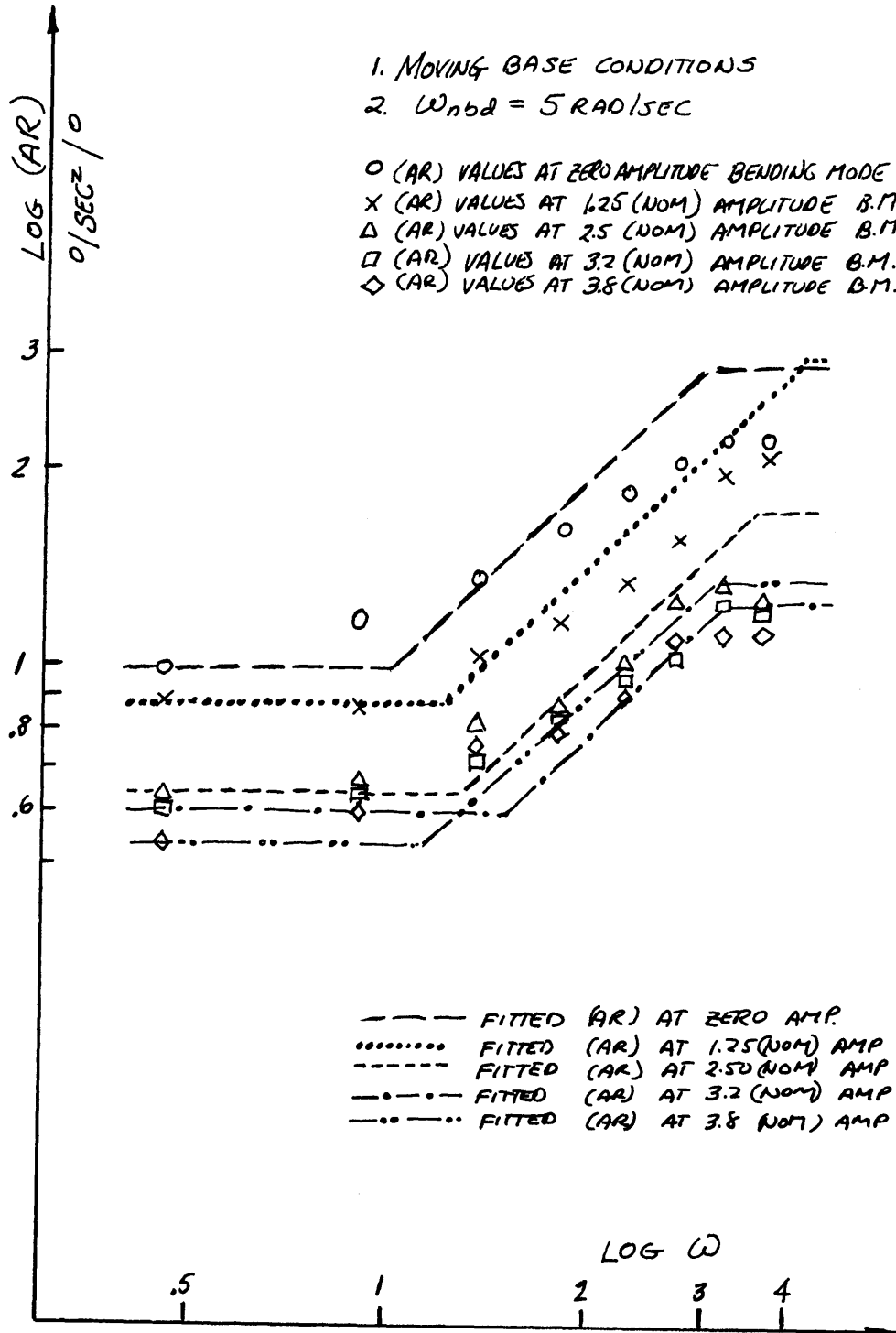
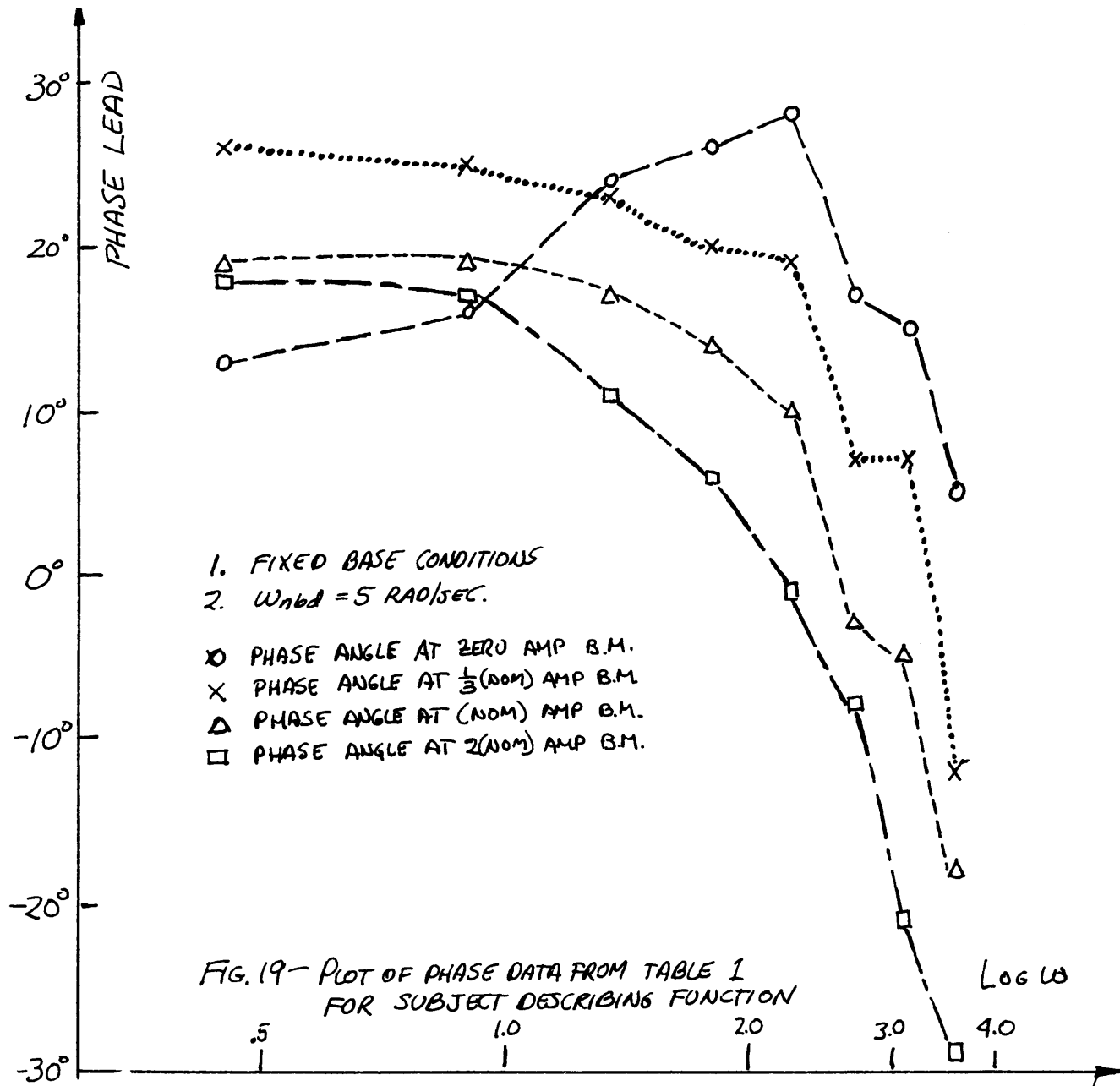
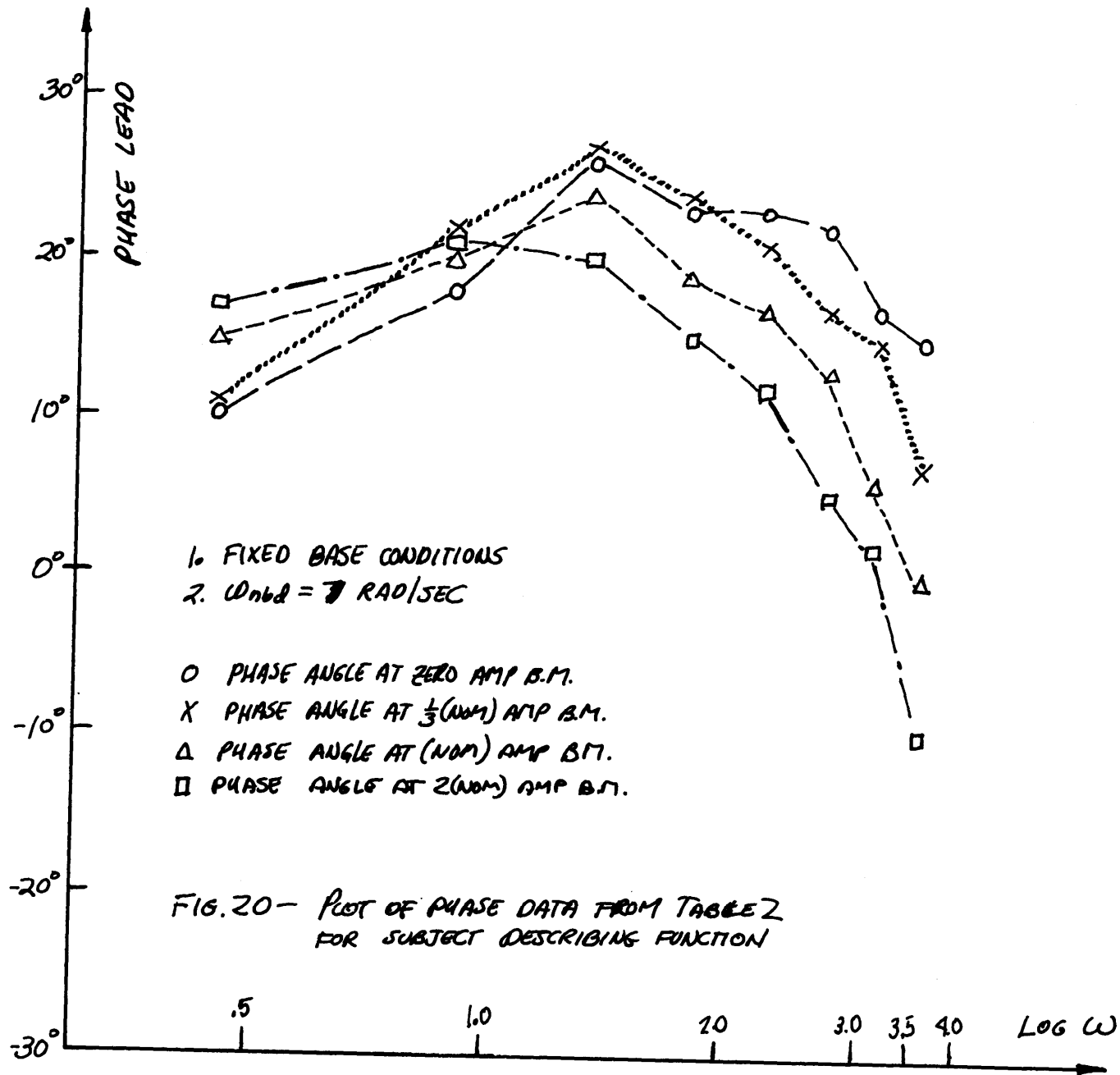
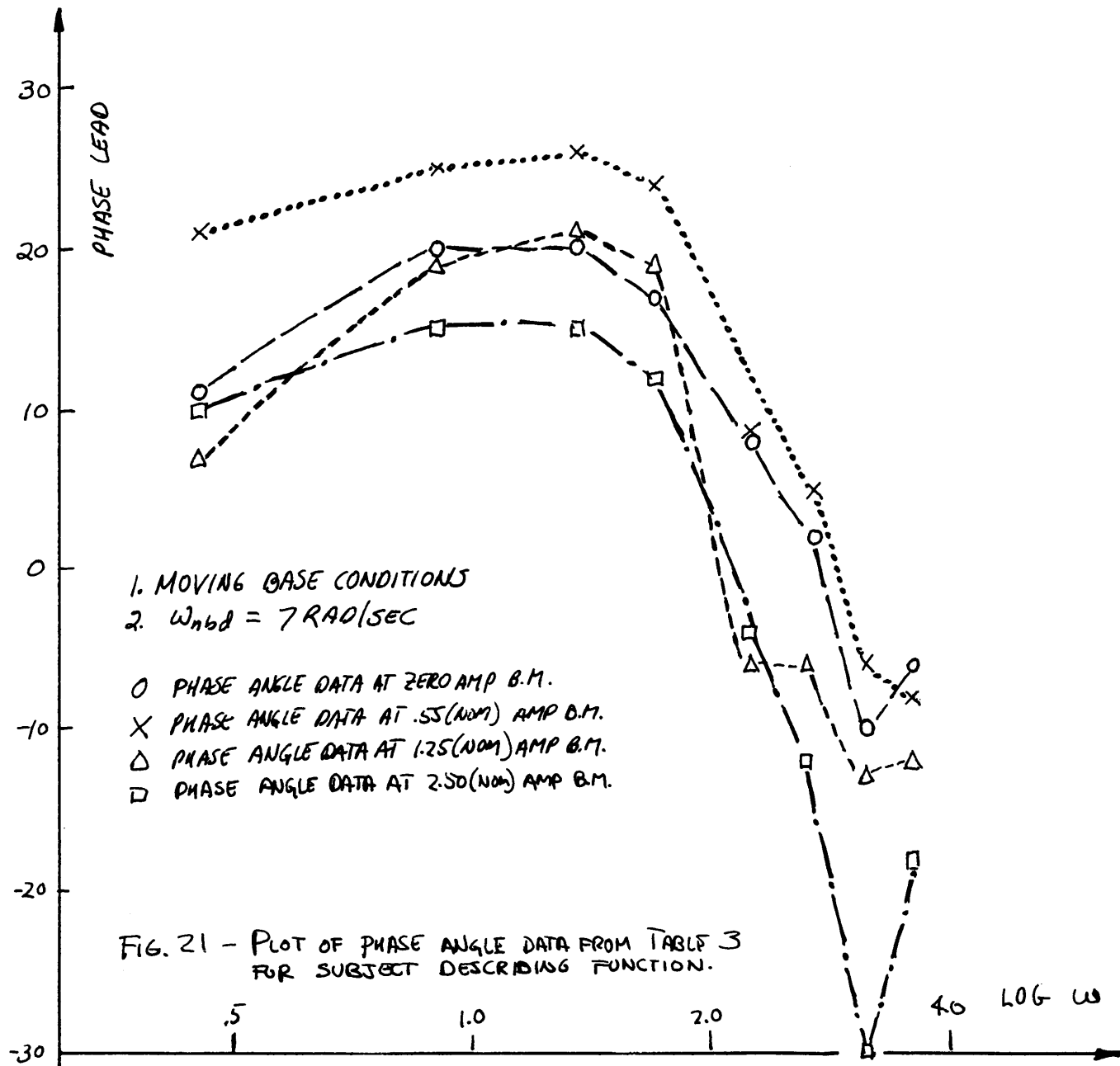


FIG. 18 - PLOT OF AMPLITUDE RATIO DATA FROM TABLE 4 FOR SUBJECT DESCRIBING FUNCTION







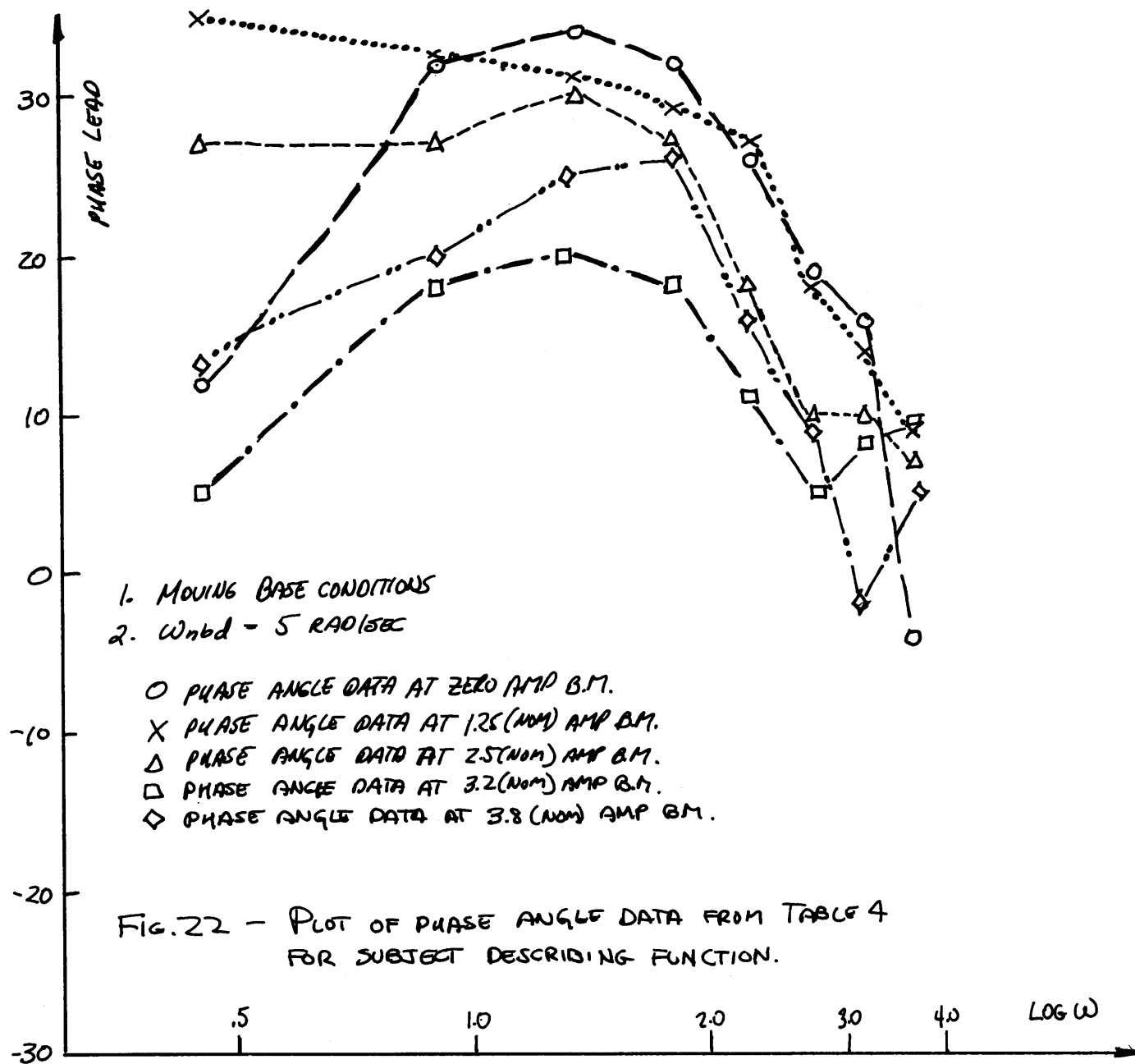


TABLE 5	
SUMMARY OF FITTED	DESCRIBING FUNCTIONS
<p>FIXED BASE, <math>\omega_{nbd} = 5 \text{ RAD/SEC}</math>            BENDING MODE AMP. = 0 :</p> $Y_p = 2.5 \frac{\left(\frac{s}{1} + 1\right)}{\left(\frac{s}{2.5} + 1\right)} e^{-.055s}$ <p>BENDING MODE AMP. = <math>\frac{1}{3} \text{ (NOM)}</math></p> $Y_p = 1.4 \frac{\left(\frac{s}{.9} + 1\right)}{\left(\frac{s}{2.7} + 1\right)} e^{-.145s}$ <p>BENDING MODE AMP. = (NOM):</p> $Y_p = .92 \frac{\left(\frac{s}{1} + 1\right)}{\left(\frac{s}{2.7} + 1\right)} e^{-.165s}$ <p>BENDING MODE AMP. = 2(NOM):</p> $Y_p = .84 \frac{\left(\frac{s}{1} + 1\right)}{\left(\frac{s}{2.7} + 1\right)} e^{-.235s}$	<p>FIXED BASE, <math>\omega_{nbd} = 7 \text{ RAD/SEC}</math>            BENDING MODE AMP. = 0 :</p> $Y_p = 2.2 \frac{\left(\frac{s}{.9} + 1\right)}{\left(\frac{s}{2.2} + 1\right)}$ <p>BENDING MODE AMP. = <math>\frac{1}{3} \text{ (NOM)}</math>:</p> $Y_p = 1.8 \frac{\left(\frac{s}{.9} + 1\right)}{\left(\frac{s}{2.3} + 1\right)} e^{-.035s}$ <p>BENDING MODE AMPLITUDE = (NOM):</p> $Y_p = 1.3 \frac{\left(\frac{s}{1} + 1\right)}{\left(\frac{s}{2.5} + 1\right)} e^{-.095s}$ <p>BENDING MODE AMP. = 2(NOM)</p> $Y_p = 1.0 \frac{\left(\frac{s}{1} + 1\right)}{\left(\frac{s}{3} + 1\right)} e^{-.145s}$
<p>MOVING BASE, <math>\omega_{nbd} = 7 \text{ RAD/SEC}</math>            BENDING MODE AMP. = 0 :</p> $Y_p = .82 \frac{\left(\frac{s}{1.1} + 1\right)}{\left(\frac{s}{3.1} + 1\right)} e^{-.145s}$ <p>BENDING MODE AMP. = .55 NOM</p> $Y_p = .78 \frac{\left(\frac{s}{1.1} + 1\right)}{\left(\frac{s}{2.9} + 1\right)} e^{-.145s}$ <p>BENDING MODE AMP. = 1.25 NOM</p> $Y_p = .64 \frac{\left(\frac{s}{1.1} + 1\right)}{\left(\frac{s}{2.9} + 1\right)} e^{-.165s}$ <p>BENDING MODE AMP. = 2.5 NOM</p> $Y_p = .58 \frac{\left(\frac{s}{1.1} + 1\right)}{\left(\frac{s}{2.9} + 1\right)} e^{-.235s}$	<p>MOVING BASE, <math>\omega_{nbd} = 5 \text{ RAD/SEC}</math>            BENDING MODE AMP. = 0</p> $Y_p = 1.0 \frac{\left(\frac{s}{1} + 1\right)}{\left(\frac{s}{3} + 1\right)} e^{-.085s}$ <p>BENDING MODE AMP. = 1.25 NOM</p> $Y_p = .88 \frac{\left(\frac{s}{1.2} + 1\right)}{\left(\frac{s}{4.2} + 1\right)} e^{-.085s}$ <p>BENDING MODE AMP. = 2.5 NOM</p> $Y_p = .64 \frac{\left(\frac{s}{1.3} + 1\right)}{\left(\frac{s}{3.5} + 1\right)} e^{-.085s}$ <p>BENDING MODE AMP. = 3.2 NOM</p> $Y_p = .60 \frac{\left(\frac{s}{1.5} + 1\right)}{\left(\frac{s}{4} + 1\right)} e^{-.085s}$ <p>BENDING MODE AMP. = 3.8 NOM</p> $Y_p = .54 \frac{\left(\frac{s}{1.1} + 1\right)}{\left(\frac{s}{3} + 1\right)} e^{-.085s}$

TABLE 6

EXPERIMENTAL CONDITIONS: FIXED BASE,  $\omega_{abd} = 5 \text{ RAD/SEC}$

ATTITUDE ERROR POWER SPECTRUM

BENDING MODE AMP.	FREQ. IN RADIANS NO. OF TRACKING RUNS AVE.	.46	.90	1.34	1.80	2.24	2.70	3.14	3.58	4.04	4.48	4.94	5.37	5.84	6.28	6.73	7.19	7.63	8.08	8.53
		0	5	920	933	981	865	578	412	307	140	62	42	31	27	18	10	9	8	4
1/3 NOM	6	2576	2510	2201	1896	1171	587	324	171	274	392	147	13	8	8	5	5	2	2	1
NOM	6	5480	4690	3583	2709	1410	608	316	268	507	565	169	13	4	7	2	5	1	4	1
2 NOM	6	6050	6243	5815	4525	2433	1044	452	473	746	778	302	28	8	7	3	5	2	2	1

SUBJECT RESPONSE POWER SPECTRUM

0	5	3990	7750	13590	17080	16185	13580	12500	7780	5000	5280	6275	5025	2895	2585	3105	3120	2265	1410	1410
1/3 NOM	6	3570	6750	11760	14625	12480	8310	6355	4635	7410	8155	2700	795	990	1050	960	615	480	465	315
NOM	6	4050	6225	9585	10125	7005	4320	3100	3405	4155	2745	570	212	330	375	330	270	225	195	165
2 NOM	6	3840	7230	12000	12915	9800	5460	2865	2770	2700	1215	195	150	195	180	135	120	105	90	75

TABLE 7

EXPERIMENTAL CONDITIONS: FIXED BASE,  $\omega_{nbd} = 7 \text{ RAD/SEC}$

ATTITUDE ERROR POWER SPECTRUM

BENDING MODE	FREQ. IN RADIANS	NO. OF TRACKING RUNS AVERAGED	.45	.90	1.34	1.80	2.24	2.70	3.14	3.58	4.04	4.48	4.94	5.37	5.84	6.28	6.73	7.14	7.63	8.08	8.53
0	5	5	1151	1056	1097	1213	940	415	192	98	54	32	19	20	18	9	7	5	5	3	2
1/3 NOM	5	5	1519	1177	1401	1488	1156	532	222	109	65	48	28	34	55	117	97	19	28	2	2
NOM	6	6	3350	2909	2860	2935	2028	837	356	200	145	93	62	106	217	320	194	58	8	4	5
2 NOM	5	5	4317	3902	3365	2976	1840	817	431	215	154	115	93	160	263	323	197	48	12	6	4

SUBJECT RESPONSE POWER SPECTRUM

0	5	5	4360	7220	13950	21100	19950	9815	5180	3560	2818	2080	1693	1990	1737	1395	1265	1030	962	826	764
1/3 NOM	5	5	3840	6330	12110	17870	17270	9580	5240	3000	2340	2175	1745	1925	1870	4570	3050	477	218	296	348
NOM	6	6	4080	6030	10630	15530	14175	7130	3720	2145	2620	1939	1329	1795	2720	2535	951	107	96	185	226
2 NOM	5	5	3675	5280	8420	10090	6710	4160	2805	1828	1845	1470	1118	1385	1500	140	318	57	70	81	85

TABLE 8

EXPERIMENTAL CONDITIONS: MOVING BASE,  $\omega_{\text{wind}} = 7 \text{ RAD/SEC}$

ATTITUDE ERROR POWER SPECTRUM

BENDING MODE AMPLITUDE	FREQ. IN RADIAN NO. OF TRACKING RUNS AVERAGED	FREQ. IN RADIAN																		
		.95	.90	1.34	1.80	2.24	2.70	3.14	3.58	4.04	4.48	4.94	5.37	5.84	6.28	6.73	7.19	7.68	8.08	8.53
0	4	9350	13200	11420	4720	1850	1180	720	410	220	130	70	60	70	100	110	60	30	20	20
.55 NOM	5	7680	12770	11220	4770	2450	1840	1080	600	270	150	100	90	90	120	160	140	90	50	30
1.25 NOM	5	10690	16030	14120	5460	2260	1970	1210	670	330	180	130	130	130	140	130	100	90	80	70
2.50 NOM	5	13550	20050	18690	8950	5110	2840	1760	720	360	210	140	140	190	300	370	370	260	200	180
		SUBJECT RESPONSE POWER SPECTRUM																		
0	4	3700	1940	1320	7980	5350	4450	4420	2340	1270	880	550	580	620	580	480	430	260	210	170
.55 NOM	5	3390	9250	11780	7800	7320	6270	3830	2410	1330	800	520	430	350	250	240	330	430	340	260
1.25 NOM	5	3470	8900	10820	6240	5100	4910	3280	1910	860	510	150	340	270	180	80	60	150	300	270
2.50 NOM	5	3800	9340	12430	8390	5770	4820	2860	1450	700	490	190	180	130	150	90	50	70	130	140

TABLE 9

EXPERIMENTAL CONDITIONS: MOVING BASE,  $\omega_{nb} = 5 \text{ RAD/SEC}$

ATTITUDE ERROR POWER SPECTRUM

BENDING MODE AMPLITUDE	FREQ. IN RADIANS NO OF TRACKING RUNS AVERAGED	.45	.90	1.34	1.80	2.24	2.70	3.14	3.58	4.04	4.48	4.94	5.37	5.84	6.28	6.73	7.19	7.68	8.08	8.53
		0	3	5230	7330	7500	4730	1930	810	550	430	290	170	110	60	60	110	110	50	40
1.25 NOM	5	7230	10900	11150	5490	2070	1660	1540	1320	790	340	120	70	50	90	90	50	40	40	30
2.5 NOM	5	9520	13490	13350	7780	3820	2940	2490	2030	1540	760	200	80	90	120	60	30	30	20	20
3.2 NOM	5	14210	18870	17890	9470	4410	2830	2990	3650	2590	940	260	90	90	110	70	30	30	20	20
3.8 NOM	4	13840	18180	16960	8790	4540	3670	2340	1560	1170	580	230	110	100	100	60	30	30	20	20

SUBJECT RESPONSE POWER SPECTRUM

0	3	3270	9240	15130	14300	8370	5690	4590	3210	2540	2180	1500	970	660	640	650	580	490	360	260
1.25 NOM	5	3640	9190	13830	9370	5600	5900	6360	6150	4030	1400	250	260	350	450	560	540	530	470	320
2.5 NOM	5	2580	6800	11000	9040	6420	6380	5740	4210	2330	710	90	120	240	320	280	250	280	270	190
3.2 NOM	5	3730	8230	10780	7730	5320	3560	6220	7120	4100	1030	90	60	140	240	250	260	280	270	250
3.8 NOM	4	3120	8000	11270	7990	6040	5850	3950	2440	1430	410	50	60	190	270	250	170	160	160	160

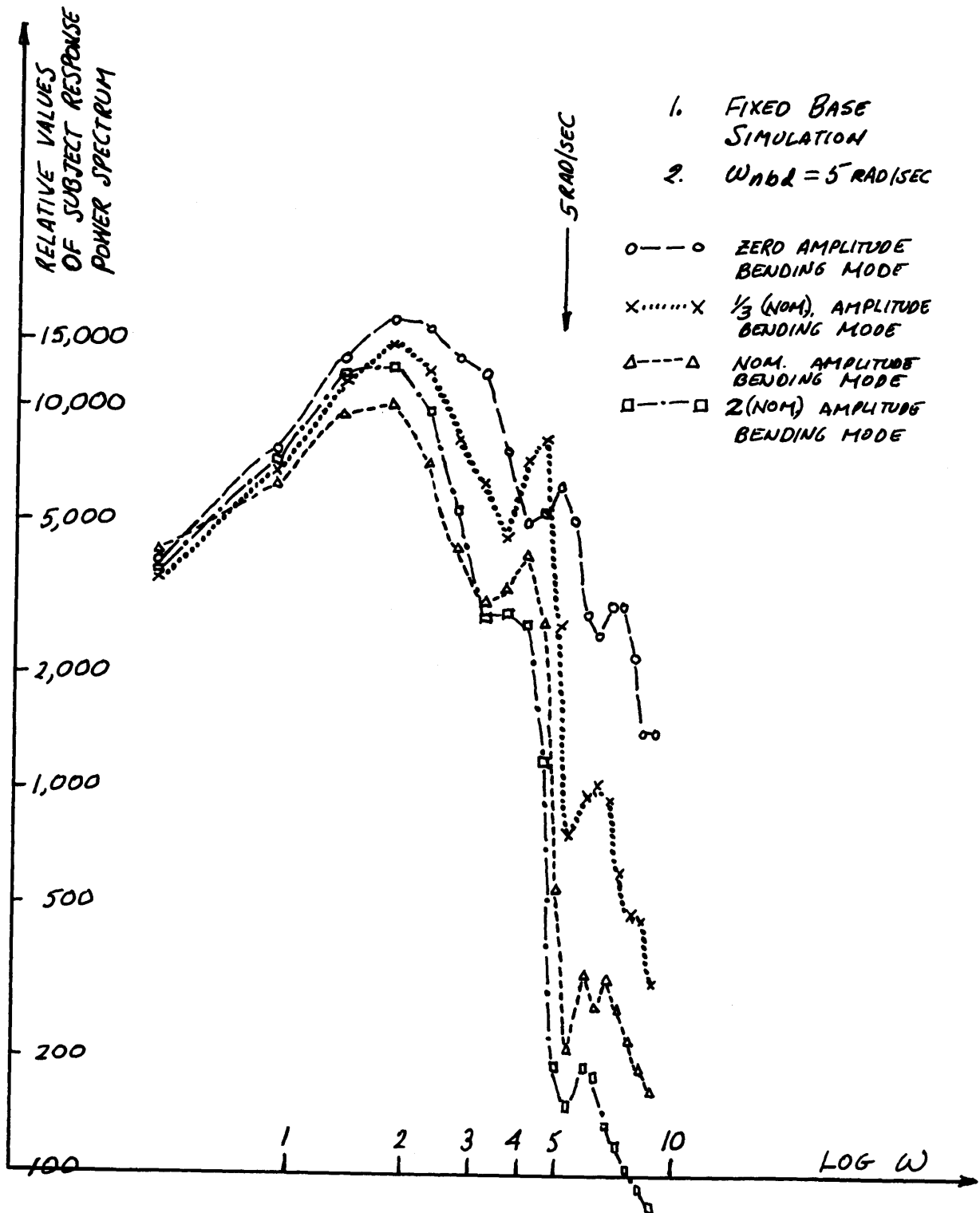


FIG 23 - PLOT OF CONTROL STICK POWER FROM TABLE 6

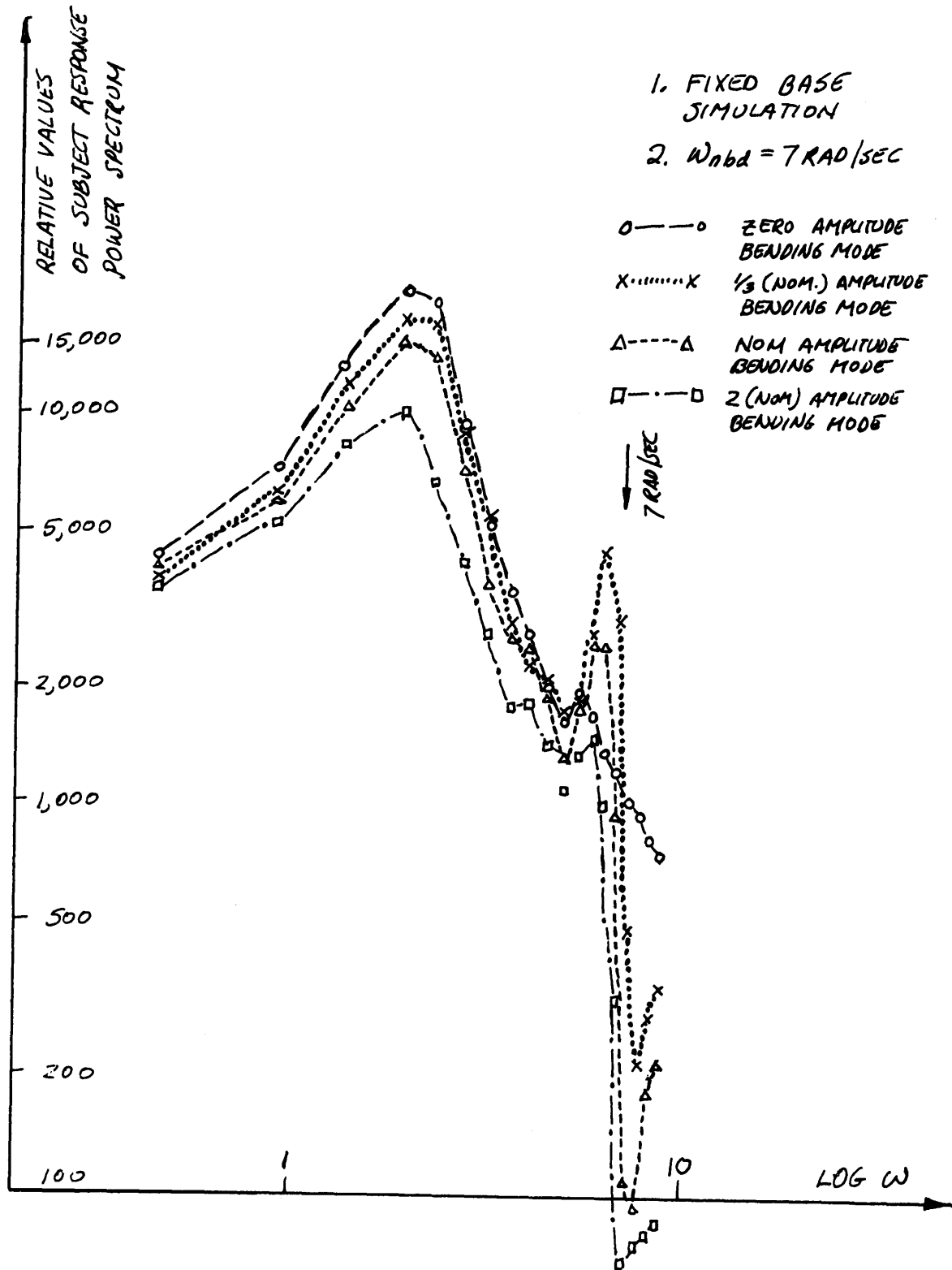


FIG 24 - PLOT OF CONTROL STICK POWER FROM TABLE 7

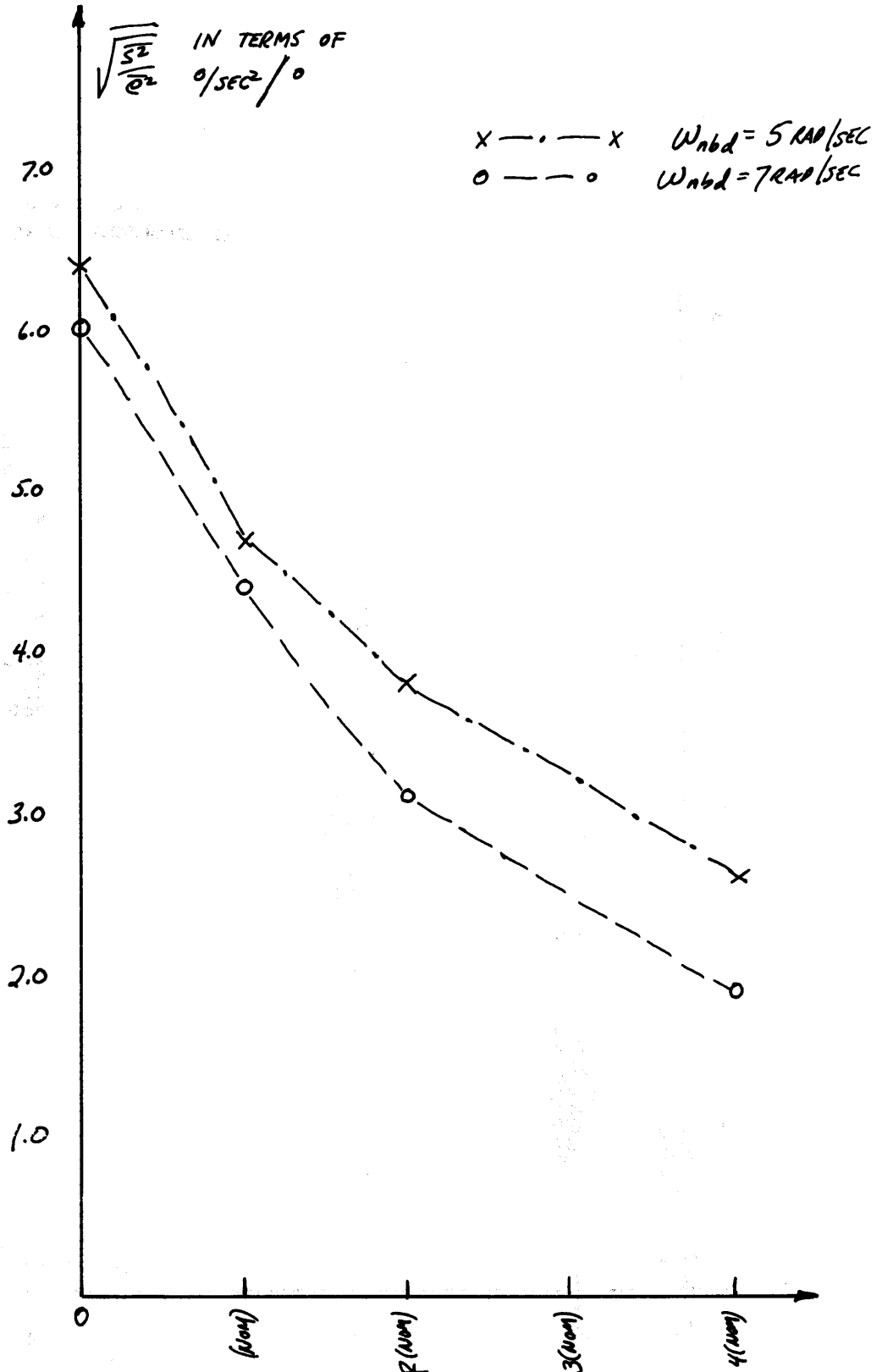


FIG 25 - PLOT OF  $\sqrt{\frac{S^2}{\omega^2}}$  VS BENDING MODE AMPLITUDE FOR FIXED BASE PLUS SIMULATED DYNAMICS

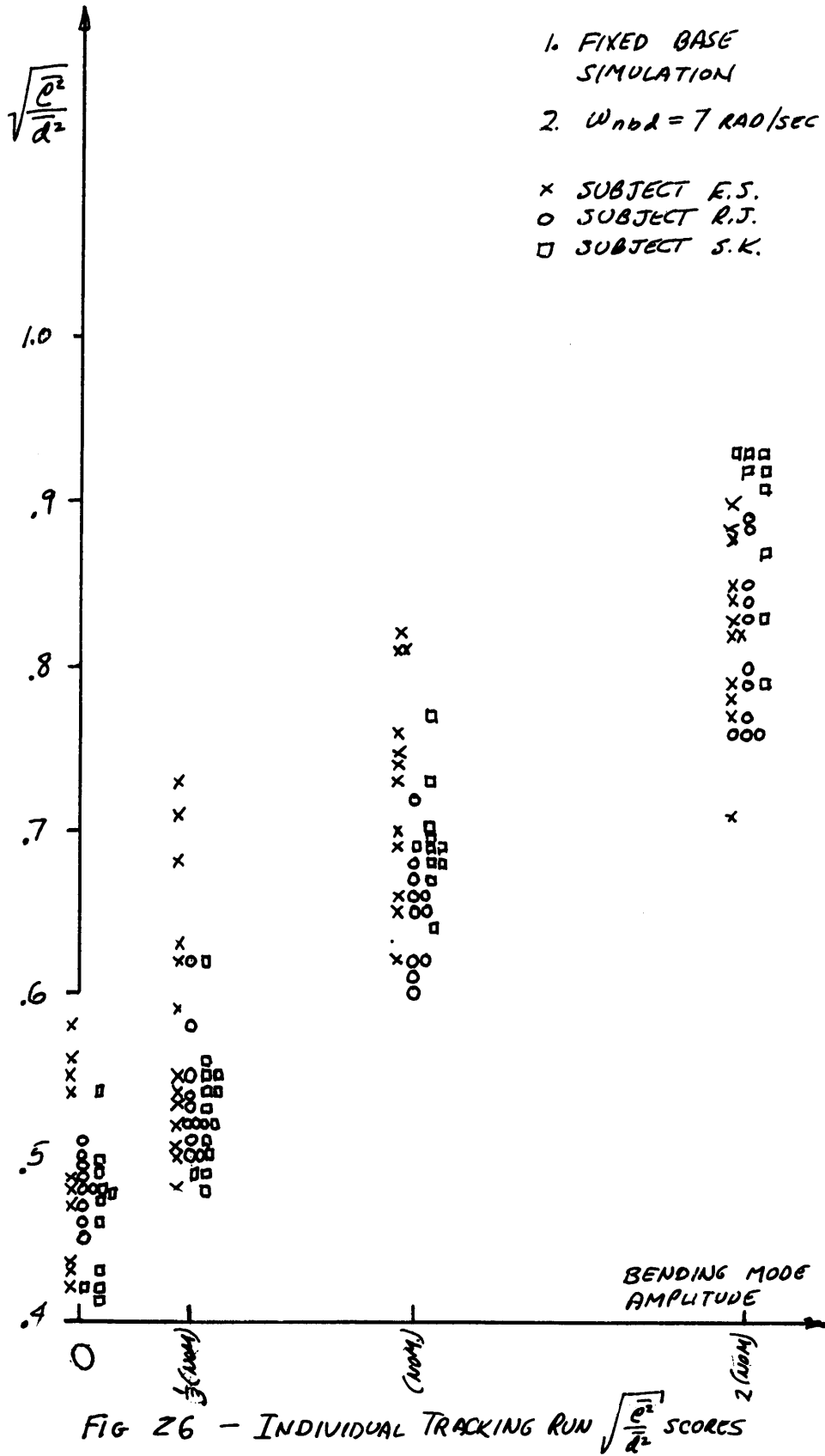


TABLE 10						
ANALYSIS OF VARIANCE FOR INTERSUBJECT EFFECTS (SEE FIG 26)						
B, M, AMP	SOURCE	SUM OF SQUARES	df	VARIANCE ESTIMATES	$F = \frac{S_b}{S_w}$	VALUE OF F FOR .05 LEVEL OF SIGNIFICANCE
0	WITHIN SESSIONS	.07	27	.003 = $S_w$	1.7	3.4
	BETWEEN SUBJECT	.02	2	.005 = $S_b$		
$\frac{1}{3}$ (NOM)	WITHIN SESSIONS	.10	34	.003 = $S_w$	3.3	3.3
	BETWEEN SUBJECT	.02	2	.01 = $S_b$		
(NOM)	WITHIN SESSIONS	.10	31	.0033 = $S_w$	3	3.3
	BETWEEN SUBJECT	.02	2	.01 = $S_b$		
2 (NOM)	WITHIN SESSIONS	.13	29	.004 = $S_w$	7.5	3.3
	BETWEEN SUBJECT	.06	2	.03 = $S_b$		

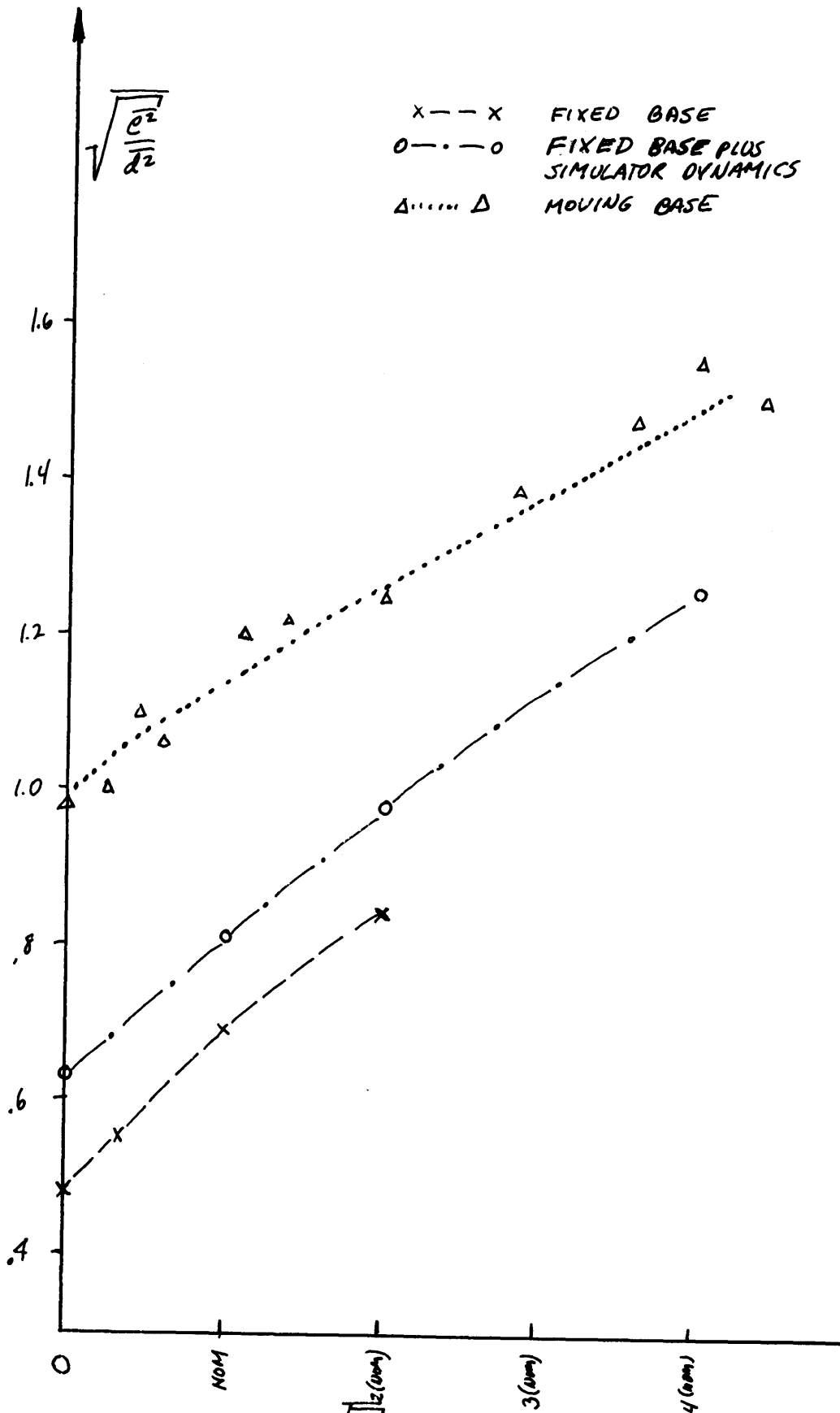


FIG. 27 - PLOT OF  $\sqrt{\frac{\dot{\theta}^2}{d^2}}$  RESULTS VS BENDING MODE AMPLITUDE FOR EACH TYPE OF SIMULATION AT  $\omega_{rod} = 7 \text{ RAD/SEC}$

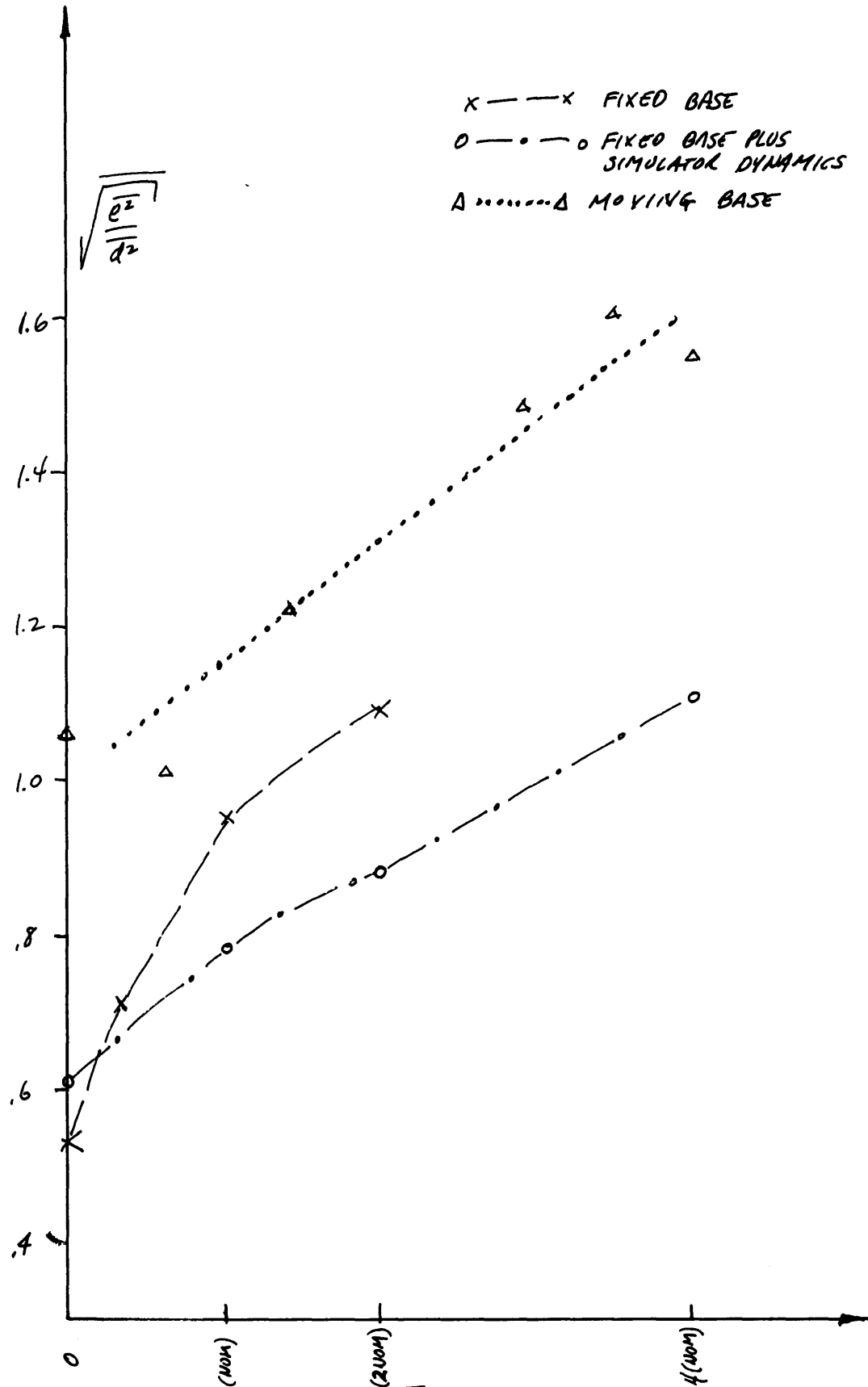


FIG 28 - PLOT OF  $\sqrt{\frac{\overline{a^2}}{d^2}}$  RESULTS VS BENDING MODE AMPLITUDE FOR EACH TYPE OF SIMULATION AT  $\omega_{wind} = 5 \text{ RAD/SEC}$

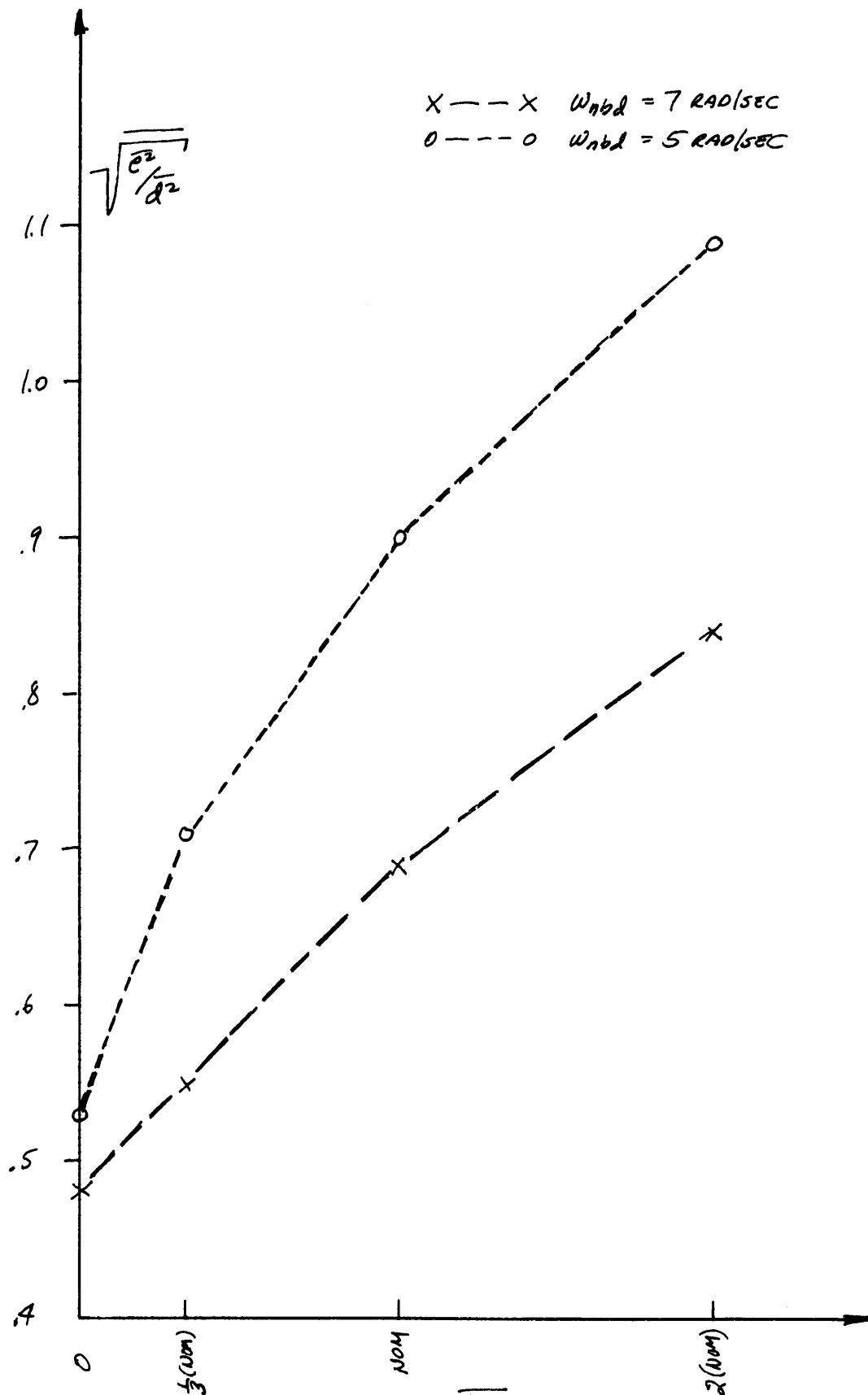


FIG. 29- COMPARISON OF  $\sqrt{\frac{e^2}{a^2}}$  RESULTS FOR  $\omega_{nbd} = 5$  AND  $7 \text{ RAD/SEC}$  DURING FIXED BASE CONDITIONS

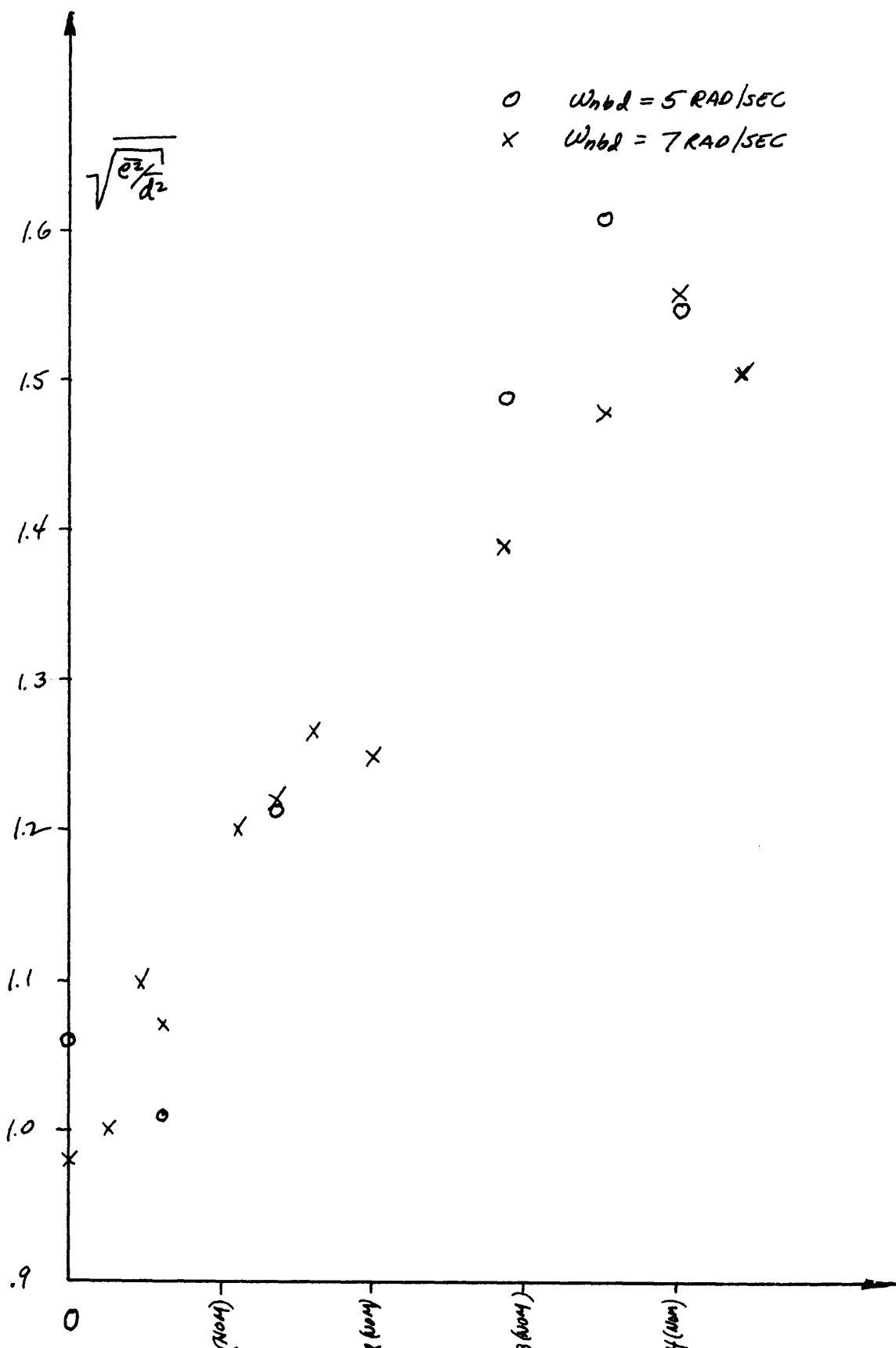


FIG 30 - COMPARISON OF  $\sqrt{\frac{e^2}{d^2}}$  RESULTS FOR  $W_{nbd} = 5$  AND  $7 \text{ RAD/SEC}$  DURING MOVING BASE CONDITIONS

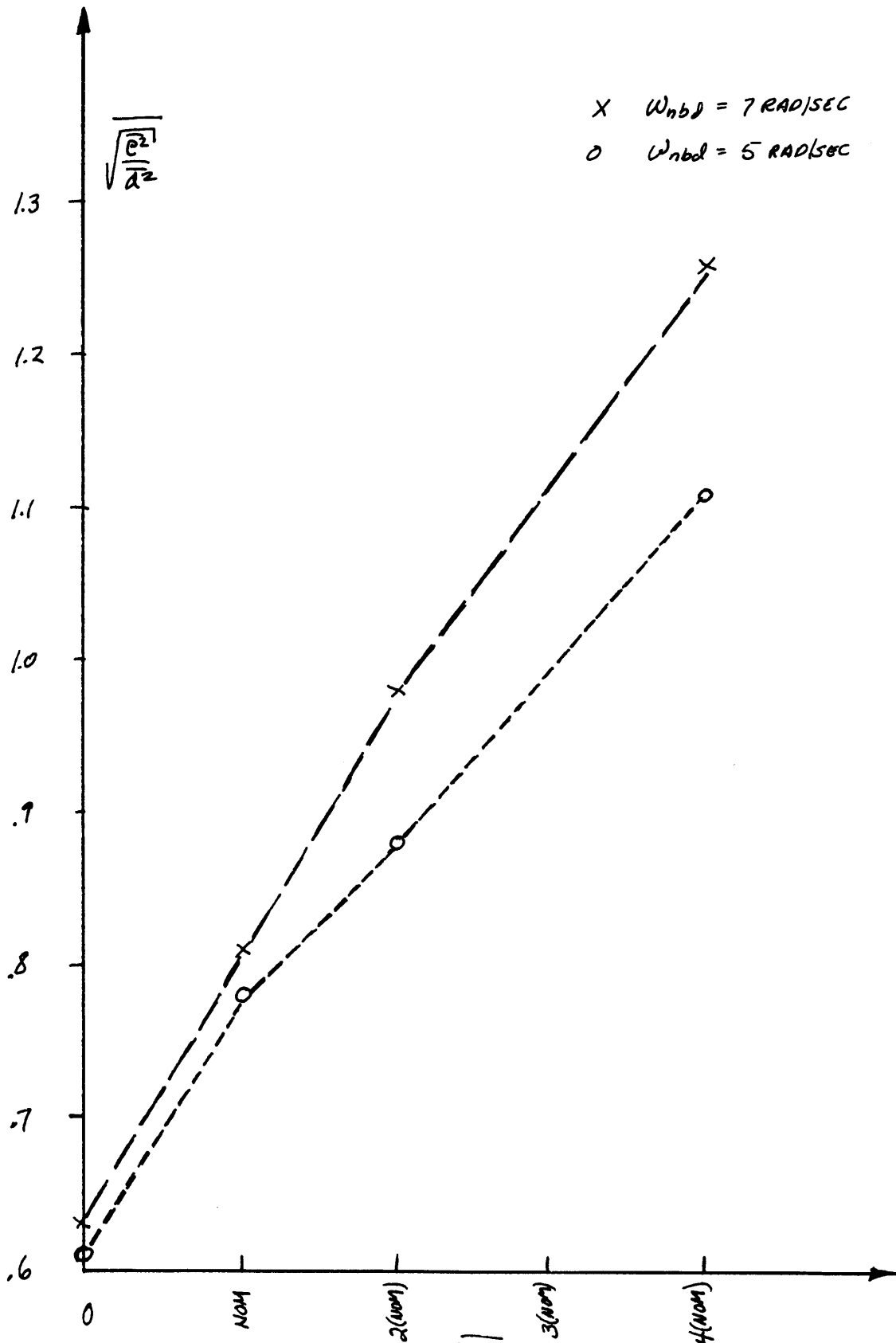


FIG 31 COMPARISON OF  $\sqrt{\frac{\theta^2}{d^2}}$  RESULTS FOR  $\omega_{nbd} = 5$  AND  
 7 RAD/SEC DURING FIXED BASE PLUS SIMULATOR DYNAMICS CONDITIONS

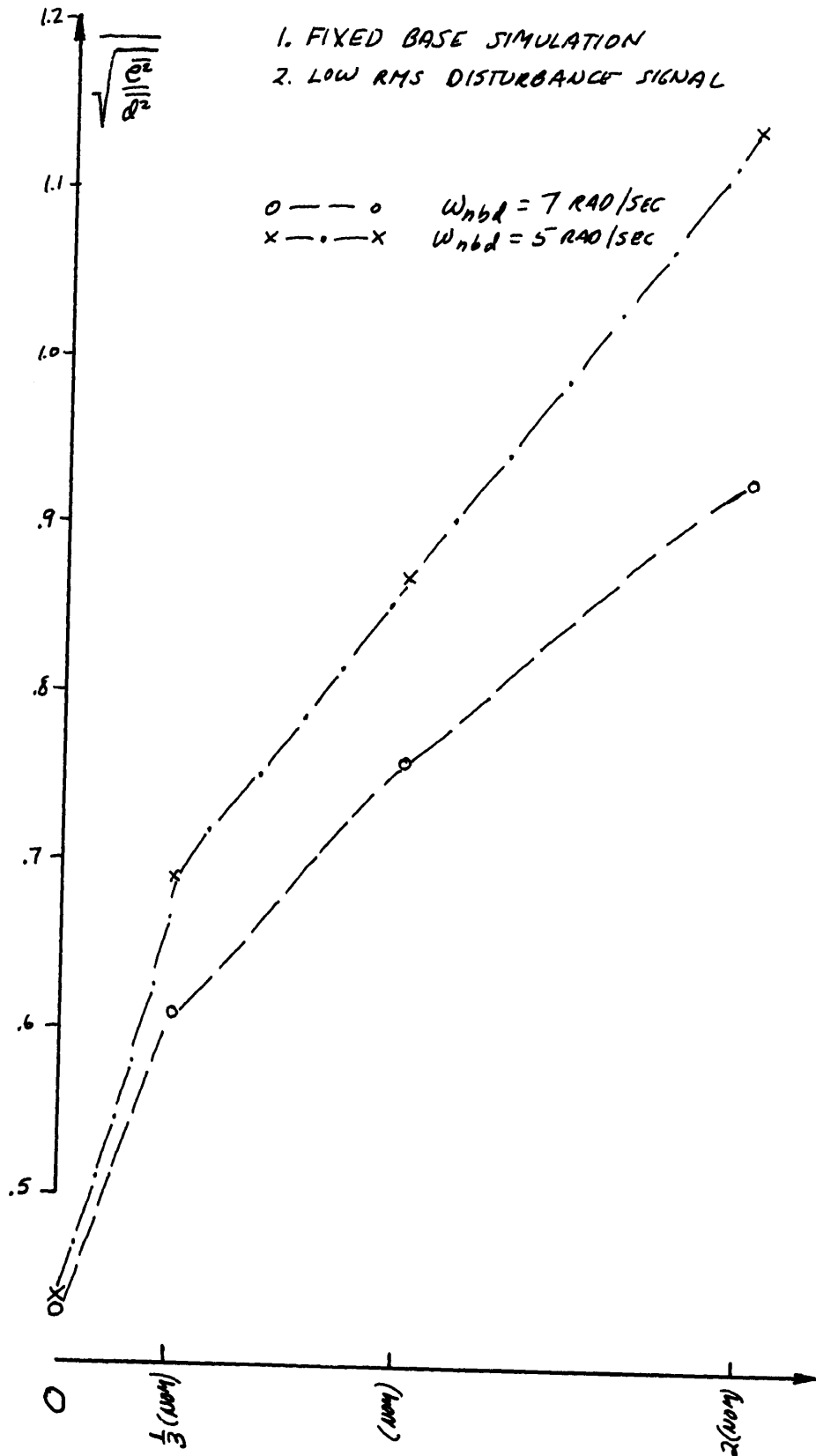


FIG. 32- PLOT OF  $\sqrt{\overline{\dot{\theta}^2}}$  VS. BENDING MODE AMPLITUDE FOR LISTED CONDITION. OF LOW RMS DISTURBANCE SIGNAL

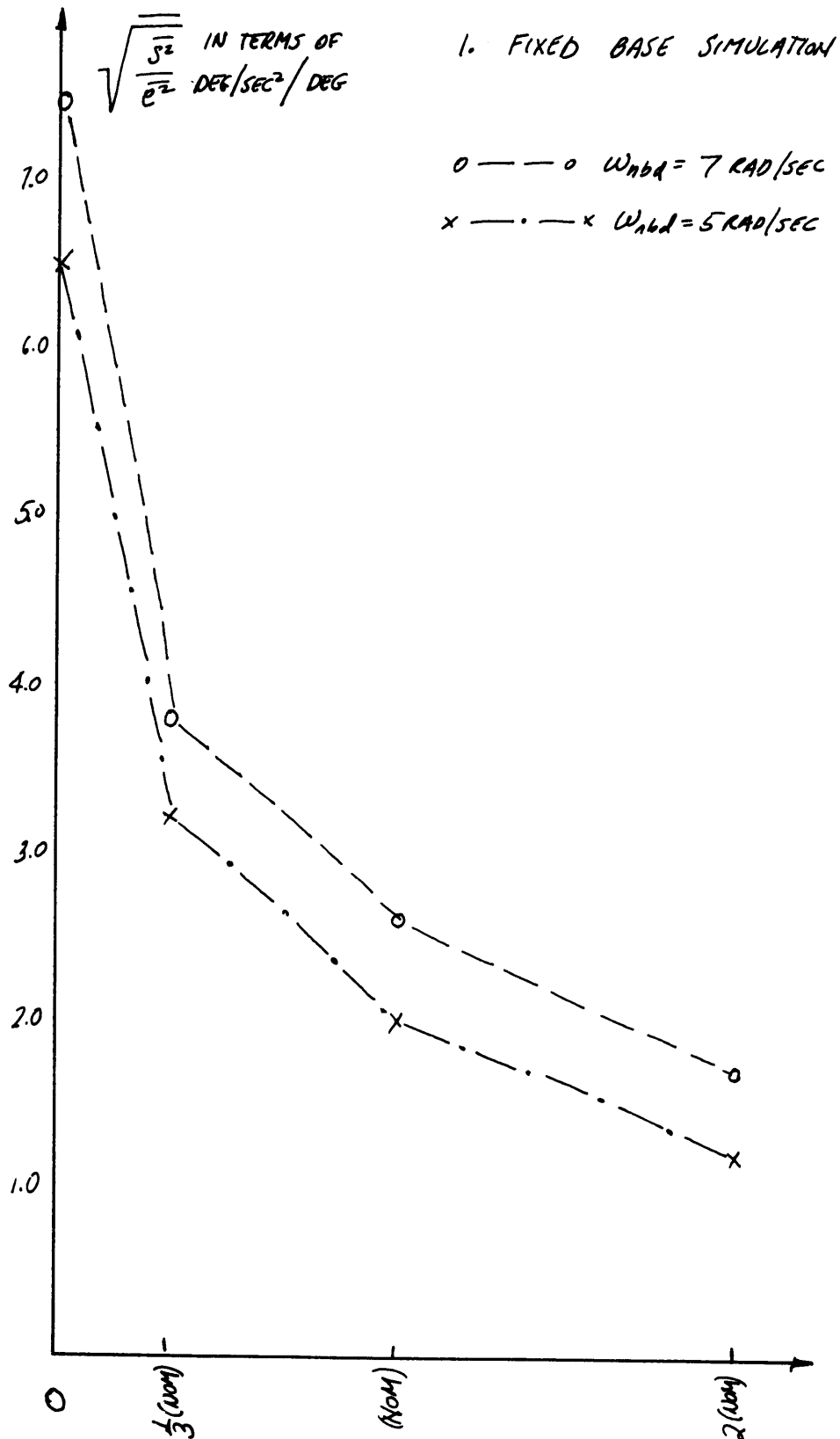


FIG 33 - PLOT OF  $\sqrt{\frac{\overline{J^2}}{\overline{\theta^2}}}$  VS BENDING MODE AMPLITUDE FOR  
CONDITION OF LOW RMS DISTURBANCE SIGNAL

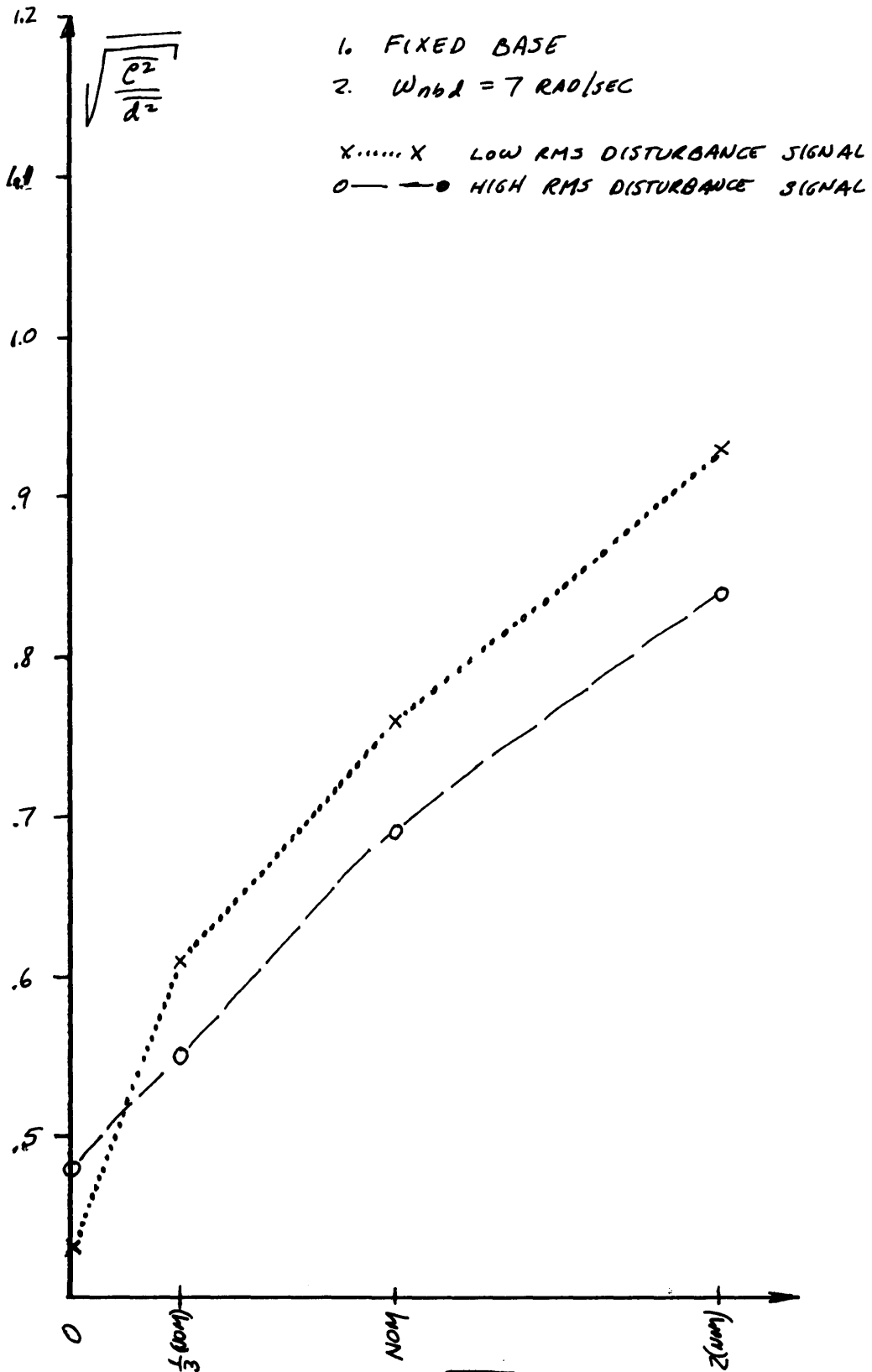


FIG 34 — COMPARISON OF  $\sqrt{\frac{\sigma^2}{d^2}}$  RESULTS FOR THE TWO DISTURBANCE SIGNALS

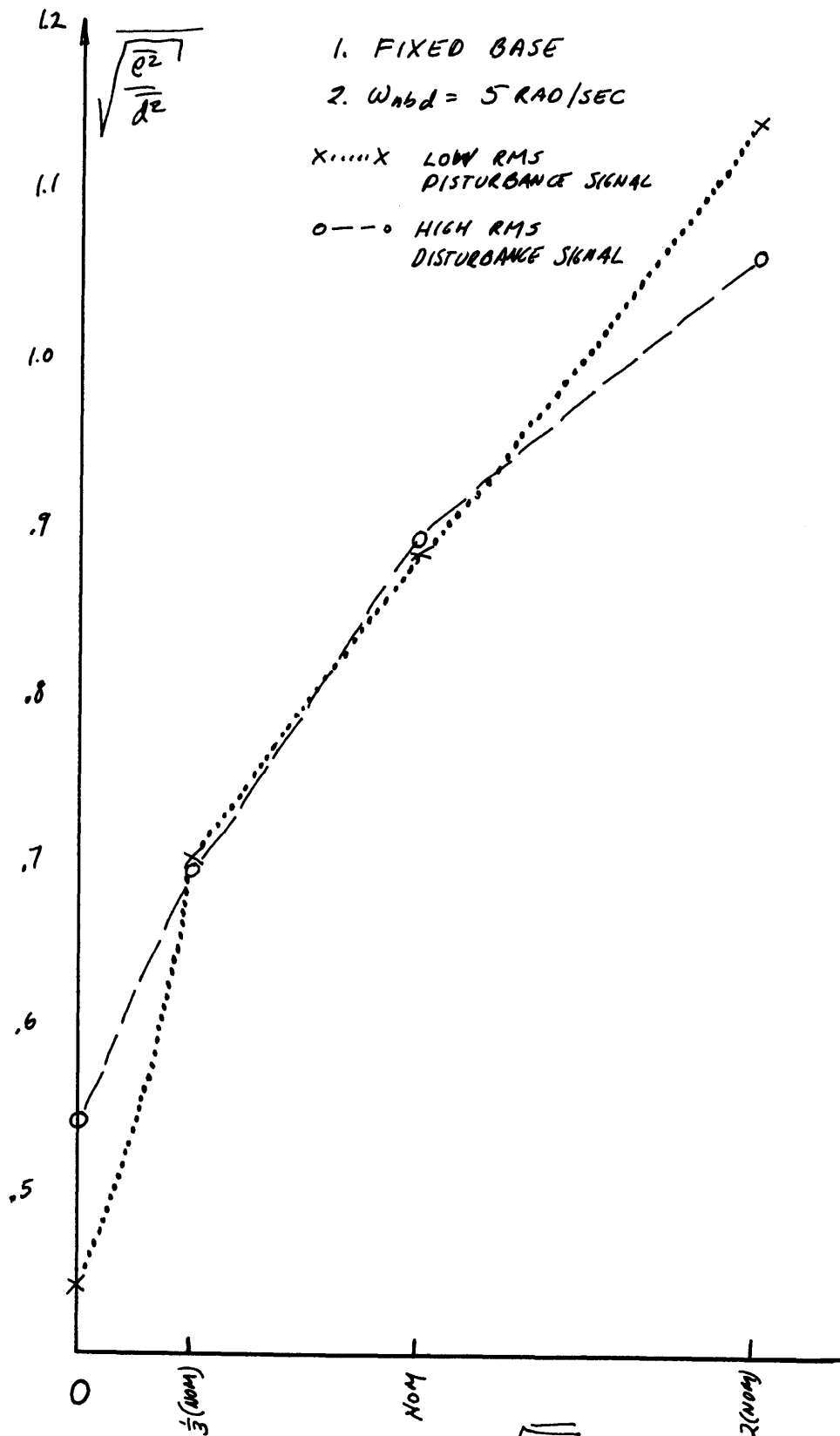
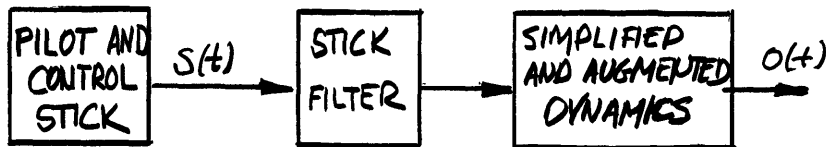


FIG 35 - COMPARISON OF  $\sqrt{\frac{\theta^2}{\Delta^2}}$  RESULTS FOR THE TWO DISTURBANCE SIGNALS



EFFECTIVE DYNAMICS FOR HARDY, GUNDERSON, & WEST VERSION:

$$\frac{O(p)}{S(p)} = \frac{(2.7)^2 (.0066)(p+7.1)(p-6.5)(p^2+(159)^2)}{(p^2+2(.5)2.7p+2.7^2)(p-.15)(p+1.00)(p^2+.01(7)p+7^2)}$$

EFFECTIVE DYNAMICS FOR SIMPLIFIED VERSION OF TEPER AND JEX PROPOSAL:

$$\frac{O(p)}{S(p)} = \frac{.5 (.0066)(p-11)(p+15.5)(p^2+(10.5)^2)}{p(p^2+2(.5)2p+2^2)(p^2+.01)7p+7^2}$$

FIG. 36

TABLE 11		
COMPARISON OF TWO SIMPLIFIED VERSIONS OF PROPOSED VEHICLE AUGMENTATION AND CONTROL STICK FILTERING SCHEMES.		
CRITERIA	TEPER AND JEX PROPOSAL	HAROY, ET AL, PROPOSAL
$\sqrt{\frac{\theta^2}{\alpha^2}}$	.86	1.20
$\sqrt{\frac{s^2}{\theta^2}}$	10.3**	2.1
$\sqrt{\frac{f_s^2}{\theta^2}}^*$	3.6** / SEC <sup>2</sup> /°	1.9°/SEC <sup>2</sup> /°

\*  $f_s$  = OUTPUT OF STICK FILTER

\*\* THESE VALUES HAVE BEEN MULTIPLIED BY 3 TO INCLUDE THE HIGHER CONTROL TORQUE GIVEN TO THIS SYSTEM.

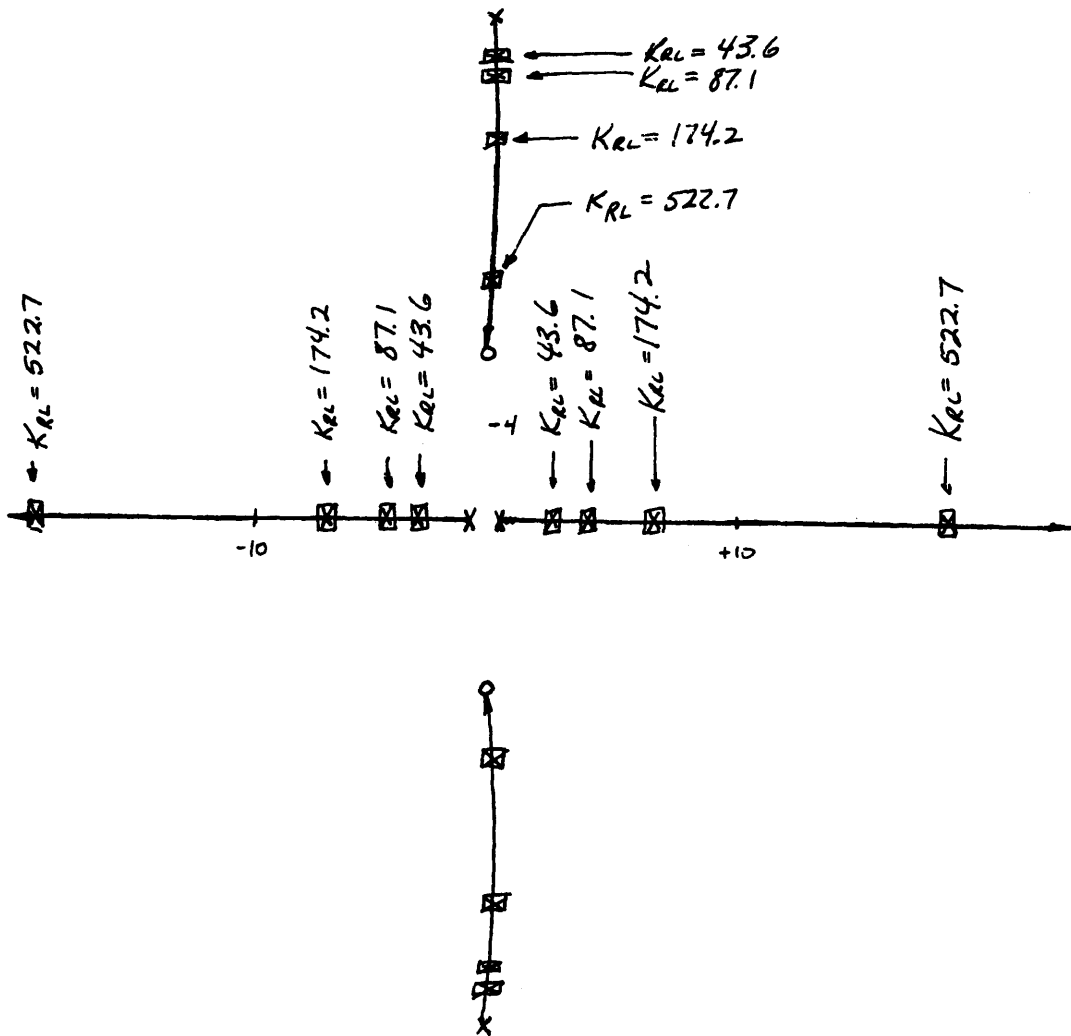


FIG. A1 - ROOT LOCUS 1  
 (DRAWN TO ONE-HALF THE SCALE DESCRIBED IN  
 APPENDIX A)

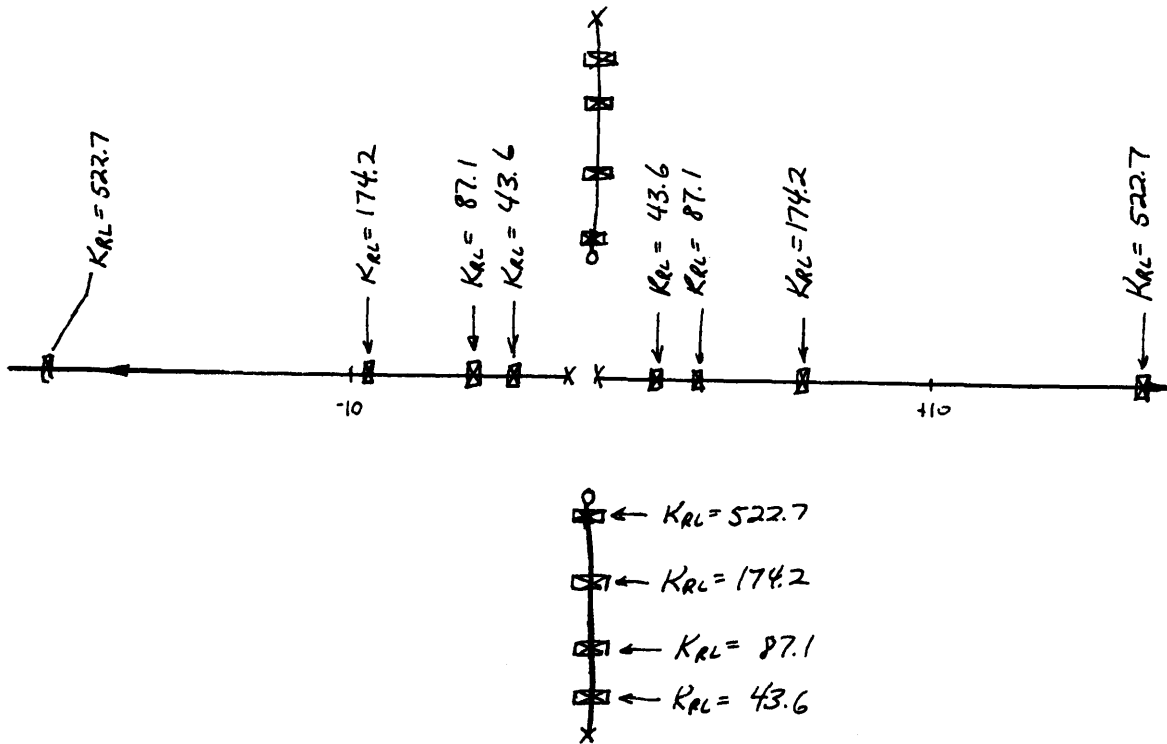


FIG A2 - ROOT LOCUS 2  
 (DRAWN TO ONE HALF THE SCALE  
 DESCRIBED IN APPENDIX A)